

This document is confidential and is proprietary to the American Chemical Society and its authors. Do not copy or disclose without written permission. If you have received this item in error, notify the sender and delete all copies.

High-pressure Methane Adsorption and Characterization of Pores in Posidonia Shales and Isolated Kerogens

Journal:	<i>Energy & Fuels</i>
Manuscript ID:	ef-2013-02466m.R2
Manuscript Type:	Article
Date Submitted by the Author:	n/a
Complete List of Authors:	Rexer, Thomas; Newcastle University, Civil Engineering and Geosciences Mathia, Eliza; Newcastle University, Civil Engineering and Geosciences Aplin, Andrew; Durham University, Earth Sciences Thomas, Keith; Newcastle University, School of Chemical Engineering and Advanced Materials

SCHOLARONE™
Manuscripts

High-pressure Methane Adsorption and Characterization of Pores in Posidonia Shales and Isolated Kerogens

Thomas F. T. Rexer, Eliza J. Mathia, Andrew C. Aplin[†], K. Mark Thomas*

Wolfson Northern Carbon Reduction Laboratories, School of Civil Engineering and Geosciences, and School of Chemical Engineering and Advanced Materials, Drummond Building, Newcastle University, Newcastle upon Tyne, NE1 7RU, UK, [†] Department of Earth Sciences, Durham University, Science Laboratories, Durham, DH1 3LE, UK

1
2
3
4
5
6
7
8
9
10
11
12
13
14
15
16
17
18
19
20
21
22
23
24
25
26
27
28
29
30
31
32
33
34
35
36
37
38
39
40
41
42
43
44
45
46
47
48
49
50
51
52
53
54
55
56
57
58
59
60

Abstract

Sorption capacities and pore characteristics of bulk shales and isolated kerogens have been determined for immature, oil-window and gas-window mature samples from the Lower Toarcian Posidonia Shale formation. Dubinin-Radushkevich (DR) micropore volumes, sorption pore volumes and surface areas of shales and kerogens were determined from CO₂ adsorption isotherms at -78°C and 0°C, and N₂ adsorption isotherms at -196°C. Mercury injection capillary pressure porosimetry, grain density measurements and helium pycnometry were used to determine shale and kerogen densities and total pore volumes. Total porosities decrease through the oil-window and then increase into the gas-window. High-pressure methane isotherms up to 14 MPa were determined at 45, 65 and 85°C on dry shale and at 45 and 65°C on kerogen. Methane excess uptakes at 65°C and 11.5 MPa were in the range 0.056-0.110 mmol g⁻¹ (40-78 scf t⁻¹) for dry Posidonia shales and 0.36-0.70 mmol g⁻¹ (253-499 scf t⁻¹) for the corresponding dry kerogens. Absolute methane isotherms were calculated by correcting for the gas at bulk gas phase density in the sorption pore volume. The enthalpies of CH₄ adsorption for shales and kerogens at zero surface coverage showed no significant variation with maturity, indicating that the sorption pore volume is the primary control on sorption uptake. The sum of pore volumes measured by a) CO₂ sorption at -78°C and b) mercury injection, are similar to the total porosity for shales. Since mercury in our experiments occupies pores with constrictions larger than ca. 6 nm, we infer that porosity measured by CO₂ adsorption at -78°C in the samples used in this study is largely within pores with effective diameters smaller than 6 nm. The linear correlation between maximum CH₄ surface excess sorption and CO₂ sorption pore volume at -78°C is very strong for both shales and kerogens, and goes through the origin, suggesting that the vast majority of sorbed CH₄ occurs in pores smaller than 6 nm. The DR micropore volume obtained from CO₂ adsorption at 0°C was 40-62% of the corresponding CO₂ sorption pore volume. Sorption mass balances using kerogen and shale isotherms showed that approximately half of the CO₂ sorption in these dry shales is in organic matter, with the rest likely to be associated with the inorganic phase (mainly clay minerals). A similar distribution was observed for supercritical CH₄ adsorption. Mass balances for adsorption isotherms for kerogen and clay minerals do not always account for the total measured sorbed CH₄ on dry

1
2
3
4
5
6
7
8
9
10
11
12
13
14
15
16
17
18
19
20
21
22
23
24
25
26
27
28
29
30
31
32
33
34
35
36
37
38
39
40
41
42
43
44
45
46
47
48
49
50
51
52
53
54
55
56
57
58
59
60

shales, suggesting that some sorption may possibly occur, which is not accounted for by the minerals identified and kerogens in the shales.

1. INTRODUCTION

Shale gas is a key methane supply resource for the future. In 2010 it accounted for 20 % of the natural gas production in the United States, up from 1 % in 2000.¹ The economic potential of shale gas reservoirs is essentially a function of the Gas-in-Place (GIP) and the rate at which that gas can be supplied from the shale matrix to an induced fracture network connected to a wellbore. At the heart of both factors is the requirement to quantify the nature of the shale pore volume and to understand how variations in pore size distributions affect the location and amounts of both sorbed and homogeneous bulk (“free”) gas.

Pore volumes and size distributions in shales are affected by compaction, maturity, grain size and mineralogy.²⁻⁷ The pore volume of shales can be determined by various techniques such as mercury injection capillary pressure (MICP) porosimetry and grain density/ helium pycnometry, scanning electron microscopy (SEM) images and gas sorption techniques, with each method characterizing a specific pore size range. Ultra small angle neutron scattering and small angle neutron scattering techniques are also useful for the determination of pore connectivity in shales.⁸⁻¹⁰ Sorbed gas in shale is in equilibrium with the homogeneous bulk gas phase (“free gas”) in larger pores. Sorption capacity depends on pressure and temperature, and structural characteristics, such as (micro-) pore volume and organic matter type, maturity and content. Supercritical methane maximum surface excess adsorption decreases linearly with reciprocal of absolute temperature for an Alum shale.¹¹ The hygroscopic moisture content of shales correlates with methane sorption capacity indicating that methane and water compete for the same sorption sites. Also, under geological conditions, moisture may be present leading to reduced methane capacity compared with dry shales.^{12,13,14}

Ross et al have reported positive correlations between maturity and sorption capacity in organic-rich shales, which they attributed to an increased micropore volume (pore width 0.3 – 2 nm).¹⁴ However, they were not able to fully explain variations in sorption capacity by micropore volume and Total Organic Carbon (TOC) content alone. Several authors have reported positive correlations of methane sorption uptake and TOC, implying that much of the sorbed methane in shale is associated with organic matter.^{12,14,15} Gasparik et al. reported no correlation for methane sorption capacity and TOC (0.8-10.5%) for dry shales¹⁶,

1
2
3 but found a correlation for another suite of dry shales with TOC (0.4-14.1%).¹³ These results
4 illustrate the complex nature of the problem when relating composition and structure of
5 shales to methane sorption capacity. Water may also be present under subsurface
6 conditions and methane adsorption studies of moisture-equilibrated shale samples show
7 that competitive adsorption has a detrimental effect on methane sorption capacity.¹³
8
9

10
11
12 The differences between surface excess and absolute amounts adsorbed become
13 significant in high pressure isotherms. The surface excess adsorbed represents the amount
14 of gas exceeding bulk gas phase density in the system. The absolute amount adsorbed
15 represents the total amount of gas molecules in the sorbed state. Various semi-empirical
16 models such as the Langmuir or the supercritical Dubinin-Radushkevich model are available
17 alongside models based on density functional theory.^{11,16,17} While the Langmuir models
18 have been commonly used to parameterize shale sorption data, the supercritical Dubinin-
19 Radushkevich model has been shown to have good applicability for a predominantly ultra-
20 microporous (< 0.7 nm) high maturity Alum shale (Ro=2.26%), for isotherms over a wide
21 temperature range (27-200°C).¹¹ Although sorption data on shales are available, the
22 absolute sorption capacity in shale remains poorly constrained.^{11-16,18-20}
23
24
25
26
27
28
29
30
31
32

33 Shales are complex heterogeneous materials with amorphous kerogen and inorganic
34 phases. The amounts of methane adsorbed on shales are also very low and this is
35 complicated by the fact that the minor kerogen component has a much larger adsorption
36 capacity than the inorganic phase in the shale. Previous studies have concentrated on the
37 correlation of surface excess with geological characterization data, for example, total
38 organic carbon, maturity etc. and this has significant limitations. The aim of this study was
39 to investigate how supercritical methane sorption capacity and pore structural
40 characteristics in shale and kerogen obtained from subcritical adsorption, change with
41 maturity. The pore structural characteristics were obtained using subcritical carbon dioxide
42 (-78 and 0°C) and nitrogen (-196°C) adsorption, mercury injection capillary pressure (MICP)
43 porosimetry, helium pycnometry and grain density measurements. Posidonia shale samples
44 from the early oil window, the oil window and the gas window were studied. The shale
45 sample set is relatively homogeneous in terms of TOC and mineral composition, allowing the
46 impact of maturity on shale and kerogen pore structure and methane capacity to be studied
47 independently of these variables. Kerogen samples were isolated using chemical methods.
48
49
50
51
52
53
54
55
56
57
58
59
60

1
2
3 Furthermore, high-pressure methane sorption isotherms were determined on both shales
4 and isolated organic kerogen matter to investigate the interrelations between high-pressure
5 sorption capacity, maturity, pore structure and the sorbed gas distribution between organic
6 and inorganic phases.
7
8
9

10 11 **1.1 Posidonia Shales**

12 The Lower Toarcian Posidonia Shale is regarded as one of the most widespread and
13 economically important petroleum source rocks of Western Europe. The formation is a
14 reference source rock of Type II kerogen.²¹⁻²³ These black shales were deposited in an
15 epicontinental sea of moderate depth, extending from the Yorkshire Basin (United Kingdom),
16 over the Lower Saxony Basin and the Southwest German Basin into the Paris Basin, during
17 the Lower Toarcian period.^{21,24,25} Recent electron microscopy studies inferred that the
18 formation of nanoporous organic materials occurred due to gaseous hydrocarbon
19 generation in Posidonia shales of gas window maturity.²⁶ Geological and geochemical
20 history has been reviewed in detail elsewhere.^{21,24-30}
21
22
23
24
25
26
27
28
29

30 31 **2 EXPERIMENTAL**

32 33 **2.1 Materials**

34 Posidonia shales were obtained from the Wickensen (WIC), Harderode (HAR) and
35 Hadessen (HAD) boreholes. These boreholes were drilled along the Western flank of the Hils
36 half-graben. The shales progressively increase in maturity from the early oil window
37 Wickensen ($R_0 = 0.53\%$), through the mid oil window Harderode ($R_0 = 0.89\%$), to the gas
38 window Hadessen ($R_0 = 1.45\%$) samples.²⁶
39
40
41
42
43

44 Carbon dioxide and nitrogen gases were obtained from BOC with purities of 99.995%
45 and 99.9995%, respectively. Methane, with a purity of 99.995%, was obtained from Air
46 Products and Air Liquide.
47
48
49

50 51 **2.2 Petrophysical characterization**

52 53 **2.2.1 Grain density measurements**

54 These measurements were carried using a glass pycnometer with nominal volume 50
55 mL. Approximately 3 g of material was crushed to < 0.5 mm particle size and dried overnight
56
57
58
59
60

1
2
3 at 105°C. The sample was added to a pre-weighed pycnometer and weighed. 10 mL of
4 surfactant (5% Teepol) solution was added and the pycnometer was filled with degassed
5 water and reweighed. Measurements were carried out using the British Standard methods
6 for calibration and use of pycnometers.³¹ Duplicate determinations were within 0.03 g cm⁻³.
7
8 Details of the method used for calculation of the grain densities are given in a previous
9 publication.¹¹
10
11
12

13 14 **2.2.2 Total Organic Carbon (TOC) Measurements**

15
16 The samples were crushed to pass through a 0.5 mm sieve. 0.1 g of the powder, in a
17 porous crucible, was treated with sufficient hydrochloric acid, 4 mol L⁻¹, to remove
18 carbonates. After the acid had drained from the crucible, the crucible and sample were
19 dried overnight at 65°C. The total organic carbon content was then measured using a Leco
20 CS244 Carbon/Sulphur Analyser.
21
22
23
24

25 26 **2.2.3 Rock Eval Pyrolysis**

27
28 Rock-Eval Pyrolysis was carried out with a Delsi Rock Eval OSA pyrolysis instrument
29 and the following parameters were measured: The S1 value is the amount of free
30 hydrocarbons in the sample and S2 is the amount of hydrocarbons generated through
31 thermal cracking of non-volatile organic matter. T_{max} is the temperature of maximum
32 release of cracked hydrocarbons. This temperature is an indicator of the maturity of the
33 sample.³²
34
35
36
37
38

39 40 **2.2.4 X-ray diffraction (XRD)**

41
42 The XRD data were obtained using a Siemens D5000 Diffractometer, using cobalt K_α
43 radiation. The samples were scanned from 2-75° 2θ, with a step time of 2 seconds per 0.02
44 degree step. The minerals were quantified by Hillier's method.^{33,34}
45
46

47 48 **2.2.5 Mercury Injection Capillary Pressure Porosimetry**

49
50 Porosimetry measurements were performed using a Micromeritics Autopore IV
51 Mercury Injection Porosimeter. Shale samples were freeze-dried for 48 h and ~ 1 cm⁻³
52 samples were loaded and outgassed under vacuum. The mercury pressure was increased
53 stepwise up to 268.9 MPa. MICP bulk volumes/densities of shale were calculated from the
54 bulk volume of the known mass of sample placed into the MICP equipment and the grain
55 density of the sample measured by the small pycnometer method. Pore volumes, measured
56
57
58
59
60

1
2
3 by injected mercury, ($MICP_{pv}$) were calculated from the difference of the volume of mercury
4 injected at 1.379 MPa and 268.9 MPa, assuming that the small amounts of mercury injected
5 at the lower pressure, only fill surface topography and micro fractures. The macro porosity
6 (1093 - 50 nm) present in some samples, which could act as methane gas storage capacity
7 was included in the total pore volume, but surface topography and micro fractures related
8 to the de-stressing and drying of geological samples were excluded (see Table 1). The
9 Washburn equation³⁵ is derived for cylindrical pores and the calculations were carried out
10 assuming a contact angle 141° between mercury and particle surface and a surface tension
11 of 0.485 N m^{-1} ,^{3,36,37} predicts that at these pressures, mercury penetrates pore throats
12 (constrictions) with equivalent diameters between 1093 nm at 1.379 MPa and 5.6 nm at
13 268.9 MPa. These diameters should be regarded as equivalent pore diameters because of
14 the variation in pore shape in the heterogeneous shale materials. Details about the
15 measurements are given in the Supporting Information (section A).
16
17
18
19
20
21
22
23
24
25

26 27 **2.3 Kerogen Isolation**

28 Shales (~25 g each) were crushed to powder and treated with 8 mL HCl (0.5 M) to
29 remove carbonates and acidified CrCl_2 (1.0 M) to remove pyrite. The mixture was diluted
30 with degassed water. The shale particles were separated from the solution by centrifuging
31 (15 min, 3500 min^{-1}). The process was repeated 3 times. Samples were then freeze-dried ($-$
32 25°C). Silicates were removed by treating the decarbonated and depyritized shales with 15
33 mL HF (0.4 M). The process was repeated twice. The shale-acid mixture was diluted with
34 degassed water and the kerogens were separated by filtering. For Harderode shales no
35 depyritization was conducted as pyrite removal proved inefficient for Wickensen and
36 Hadessen shales. XRD profiles were obtained before and after the demineralization to
37 ensure removal of all minerals except pyrite. Details about the process and chemical
38 reactions are given in Supporting Information (Section B1). The isolated kerogen samples
39 contained varying amounts of pyrite (see Supporting Information, Section B2, Figure S1),
40 which were measured by proximate analysis (see Section B3 and Table S1). CO_2 (-78°C) and
41 N_2 (-196°C) adsorption isotherms for pyrite showed that no significant adsorption occurred
42 (see Supporting Information, Figure S2). Therefore, all kerogen adsorption isotherms were
43 corrected for pyrite content (Supporting Information, Section B3).
44
45
46
47
48
49
50
51
52
53
54
55
56
57
58
59
60

2.4 Pore characterization by low-pressure sorption

Adsorption characteristics of nitrogen and carbon dioxide on the shales and kerogens were investigated using an Intelligent Gravimetric Analyzer (IGA), supplied by Hiden Isochema Ltd., Warrington, UK. The system has been described in detail previously.¹¹ Sorption measurements on shale by IGAs at temperatures above 0°C require removal of traces of moisture from the gas supply. Details of system modifications for moisture-removal from the gas stream are given in Supporting Information (section C2).

Adsorbent samples were crushed to particle sizes between 500 – 1180 μm , loaded (130 – 160 mg of shales, 40-105 mg of kerogens) in the IGA and out-gassed to a constant weight (typically for ~ 4 hours), at $< 10^{-4}$ Pa, at 110°C. N_2 isotherms were measured at -196°C up to a pressure of 99 kPa. CO_2 isotherms were collected at -78°C and 0°C up to 100 kPa. The saturated vapor pressure (p_0) for CO_2 at 0°C is 3.49 MPa. All adsorption isotherms were measured a minimum of two times and the experimental repeatabilities were typically ± 1.5 % for CO_2 adsorption uptakes at both -78 and 0°C at 0.1 MPa and ± 1.1 % for N_2 uptakes at -196°C and 0.099 MPa.

2.5 High-pressure methane sorption

High pressure methane isotherms were measured on a Hiden Isochema Intelligent Manometric Instrument (IMI). System specifications are described in Supporting Information (see Table S2). Crushed shale samples (500 – 1180 μm) and kerogens were pre-dried (typically for ~ 4 hours, at < 500 Pa and at 110°C) in a vacuum oven and loaded (typically ~ 10 g shale, 0.8-1.3 g kerogen) into the IMI sample cell. For kerogens, displacers were employed to reduce the void volume, because only relatively small quantities were available. Prior to the measurements another internal drying was carried out (typically for ~ 4 hours), at $< 10^{-4}$ Pa, at 110°C followed by helium pycnometry (2 MPa dosing pressure at 40°C and ca. 0.7 MPa at equilibrium after dosing) to determine the skeletal volume. The assumption is that helium penetrates all accessible porosity.³⁸

Methane isotherms were measured at 45, 65 and 85°C. In between measuring isotherms the system was out-gassed below $< 10^{-6}$ Pa and heated to 110°C. Excess uptake was calculated by a mass balance given in Supporting Information (Section D1). Isotherm experimental repeatabilities were typically ± 5.0 % for both shale and kerogens at 10 MPa.

1
2
3 In addition, assuming that helium adsorption is negligible, helium isotherms were measured
4 at all temperatures as blank determinations for no adsorption, to leak-test the system and
5 to monitor skeletal densities.
6
7

8 9 **2.6 Saturated vapor pressure**

10 Saturated vapor pressures (p_0) and gas densities were calculated from the NIST
11 Standard Reference database 23 by using the REFPROP Version 9.0 software.³⁹ The following
12 equations of state (EOS) were used: CO₂ (Span et al)⁴⁰, N₂ (Span et al)⁴¹, CH₄ (Setzmann et
13 al)⁴² and helium (Lemmon et al)³⁹.
14
15
16
17
18

19 **3 RESULTS**

20 **3.1 Petrophysical characterization**

21 **Total Organic Carbon and Grain densities**

22 The TOC and the grain densities obtained from both buoyancy and helium
23 pycnometry are shown in Table 1. TOC values range from 5.8 - 10.9 wt%. Excellent
24 agreement was observed for shale grain densities (2.331 – 2.607 g cm⁻³) and helium
25 pycnometry (2.297 - 2.614 g cm⁻³) with measurements for specific samples agreeing within
26 3%. Kerogen densities were much lower and ranged from 1.024 to 1.368 g cm⁻³.
27
28
29
30
31
32
33
34
35

36 **Rock Eval Pyrolysis**

37 The bulk geochemical data classifies the Posidonia Shale kerogen as Type II with a
38 maturation trend typical for the marine algal kerogen (see Table 2).⁴³ The Rock-Eval analyses
39 showed a decrease of hydrogen index (HI) from ~700 mg HC/g in the early oil window down
40 to ~370 mg HC/g in the peak oil window and 50 mg HC/g in the gas window. The S1 and S2
41 parameters decrease with increasing maturity.
42
43
44
45
46
47

48 The Rock Eval data for the kerogens shows that the T_{max} values are slightly lower than
49 for the corresponding shales (see Table S1b) with the difference increasing with increasing
50 kerogen maturity. Heat and mass transfer effects are likely to be quite different for isolated
51 kerogens and kerogens embedded in an inorganic shale matrix and these factors will
52 influence T_{max} significantly. However, good linear correlations are observed for S2 peak ($R^2 =$
53 0.9595) and HI ($R^2 = 0.9977$) parameters for pyrolysis of the kerogen and shales (see Figures
54
55
56
57
58
59
60

1
2
3 S1c and d). Previous work has shown that S2 and HI parameters are decreased by mineral
4 matrix effects involving retention of pyrolysis products.⁴⁴ Therefore, it is reasonable to
5 conclude that the kerogen isolation process only had a minimal effect on kerogen
6 properties.
7
8
9

10 **Mineralogy**

11
12 The bulk mineralogical compositions of these Posidonia samples are similar
13 throughout the whole maturation sequence (see Table 3). The most abundant phases are
14 calcite (31-55 wt.%) and phyllosilicates (23-37 wt.%). Within the phyllosilicates group, illite-
15 rich mixed layer illite-smectite is the most prominent component, followed by kaolinite,
16 illite, muscovite and chlorite. In addition, there is a moderate content of quartz (8-16 wt.%)
17 and minor contents of pyrite (4-9 wt.%), feldspars (1-5 wt.%) and dolomite (0.3-6.4 wt.%).
18 Other minerals include siderite, marcasite and anatase, but their content does not exceed 2-
19 3 wt.%. The XRD and microscopic data classify the immature Posidonia Shale as a
20 calcareous nanoplankton-, silt- and clay-bearing mudstone.
21
22
23
24
25
26
27
28

29 **3.2 Pore characterization**

30 **3.2.1 Total Pore Volume (TPV) and MICP Pore Volume (MICP_{pV})**

31
32 The bulk volume obtained from MICP and the skeletal densities from grain density
33 measurements and helium pycnometry were used to calculate the total pore volumes of the
34 Posidonia shales. The total pore volume (< 1093 nm) was obtained from mercury injection
35 at 1.379 MPa and the helium or grain densities. Mercury injection measures the accessible
36 pore volume for constrictions with equivalent pore widths > 5.6 nm based on the prediction
37 of the Washburn equation for the pressure (268.90 MPa) used. Correcting for
38 conformance/surface roughness using the method of Wang et al³, which, depending on the
39 sample, ranged from 1.379 - 35.2 MPa mercury pressure (corresponding to equivalent pore
40 diameters of 43 to 1093 nm), did not lead to significantly different MICP pore volumes. The
41 maximum pore sizes in the samples obtained from MICP were as follows: WIC7145 (156 nm),
42 WIC7155: (156 nm), HAR7038 (21 nm), HAR 7060 (24 nm), HAD 7090 (156 nm) and
43 HAD7199 (547 nm). These maximum pore sizes decrease through the oil-window and then
44 increase into the gas-window.
45
46
47
48
49
50
51
52
53
54
55
56
57
58
59
60

Mercury injection volumes were ~80% of total pore volumes in the Wickensen samples, ~40% in the Harderode samples and 50-75% in the Hadessen samples. Total pore volumes and mercury injection volumes show the same trend with maturity (see Table 4). There is a decrease in total pore volume from around of 65 to 15 mm³ g⁻¹ for the Wickensen samples (R₀=0.53%) to the Harderode samples (R₀=0.89 %) and an increase back to about 55 mm³ g⁻¹ for Hadessen (R₀=1.45%) shales. A similar trend of pore volume with maturity, with a minimum in the oil window, has been observed previously for coals.⁴⁵

3.2.2 Sorption Pore Volumes

According to the Gurvitch Rule adsorption uptake at $p/p_0 \approx 1$ when expressed as a volume of liquid, using the liquid density should be the same for all adsorptives on a given adsorbent.⁴⁶⁻⁴⁸ These sorption pore volumes can thus be calculated from CO₂ isotherms at 0.1 MPa and -78°C or nitrogen adsorption isotherms at 0.1 MPa and -196°C.

Carbon dioxide isotherms for both shales and kerogens at -78°C do not reach plateaus and are therefore classified as Type I/II in the IUPAC Classification Scheme (see Figures 1 and 2).⁴⁹ Maximum uptake (at $p/p_0 \approx 1$) was 0.23 – 0.44 mmol g⁻¹ on shales and 1.83 – 3.02 mmol g⁻¹ on kerogens (see Figure 1 and 2). Tabulated isotherm data are given in Supporting Information, Table S4. Normalizing the isotherms by maximum uptake reveals that all isotherms (shale and kerogen) have very similar isotherm shapes. This indicates that the Posidonia shales and kerogens have similar pore size distributions within the porosity range measured by CO₂ adsorption at -78°C.

Calculated sorption pore volumes from CO₂ isotherms at -78°C (CO₂ SPV) of shale and kerogen are shown in Table 4. An adsorbed phase density of 1.177 g cm⁻³ was assumed. There is a range of possible values for densities of adsorbed CO₂ from 1.562 g cm⁻³ for solid at -78°C to 0.762 g cm⁻³ at 21.1°C. The density chosen is in the middle of this range and is the liquid density of CO₂ at the boiling point (-56.6°C).³⁹ CO₂ sorption pore volumes range from 8.3 to 16.4 mm³ g⁻¹ on shale and from 68.5 to 113.0 mm³ g⁻¹ on kerogen (see Table 4). There is a trend in sorption and MICP pore volumes with maturity with the minimum observed for HAR shales. The sum of the CO₂ sorption pore volumes and MICP pore volumes are very similar to the corresponding total pore volumes calculated from the MICP bulk volume (< 1093 nm) and the grain or helium density with a linear correlation coefficient

1
2
3 with $R^2 > 0.97$ (see Figure 3). Therefore, the CO_2 sorption pore volume and MICP pore
4 volume (5.6 – 1093 nm) account for the total pore volume (< 1093 nm) in this suite of shale
5 samples. Considering that the Washburn equation is derived using cylindrical pores and
6 predicts that mercury penetrates pore constrictions down to effective pore diameters of
7 approximately 5.6 nm, the good agreement suggests that the CO_2 sorption pore volume
8 accounts for pores up to approximately this pore diameter. This sorption pore volume
9 represents approximately 25% of total pore volume in the Wickensen samples, 46 and 66 %
10 in the Harderode samples and around 21 and 32% in the Hadessen samples (see Table 4).
11 However, we note that the high pressures used in mercury injection porosimetry may
12 distort shale samples. Furthermore, MICP measurements were carried out on 1 cm^3 chips
13 while sorption measurements were carried out on particles (500 – 1180 μm) and, thus, the
14 accessible pore volume may differ.
15
16
17
18
19
20
21
22
23
24

25 Nitrogen adsorption isotherms of shales and kerogen at -196°C are shown in Figures
26 4 and 5, respectively. Tabulated isotherm data are given in Supporting Information, Table S5.
27 Nitrogen uptakes on Harderode shales were too low to allow measurements of isotherms.
28 This is in contrast to the CO_2 isotherms for the Harderode shales at -78°C , which, although
29 having the lowest uptake, have isotherm shapes consistent with the other samples. This
30 difference in isotherm uptake is attributed to activated diffusion effects for N_2 in
31 ultramicroporosity at -196°C , which is not apparent for CO_2 adsorption at -78°C .^{50,51} The
32 shapes of the N_2 adsorption isotherms indicate micropore filling (up to $p/p_0 \approx 0.2$) and
33 gradual increase for $p/p_0 > 0.2$ and increased upward isotherm curvature close to $p/p_0 = 1$.
34 Maximum uptakes at $p/p_0 \approx 1$ were in the range $0.22 - 0.59 \text{ mmol g}^{-1}$ on shale and $0.32 -$
35 4.0 mmol g^{-1} on kerogen (see Table S5). Steep uptake of nitrogen isotherms of Hadessen
36 shales and kerogens at -196°C at very low p/p_0 ($p/p_0 < 0.02$) indicates filling of
37 ultramicropores.⁵²
38
39
40
41
42
43
44
45
46
47
48

49 Surface Areas calculated from the BET isotherms are given in Table 4. Since some
50 activated diffusion effects were observed for N_2 adsorption on HAR shales and kerogens at $-$
51 196°C , the surface areas were not suitable for comparisons between samples.
52
53
54
55
56
57
58
59
60

3.2.3 Micropore Volumes

Some authors favor the use of carbon dioxide adsorption at 0°C for the characterization of the microporous structure in activated carbons and coals, because, compared with N₂ at -196°C, the higher temperature for CO₂ adsorption overcomes kinetic limitations due to activated diffusion.^{50,53,54} Carbon dioxide isotherms at 0°C of shale and kerogen are Type I Isotherms (see Supporting Information Table S3 for tabulated data). At these temperature and pressure conditions (< 0.1 MPa), CO₂ sorption is limited to ultramicropores (< ~0.7 nm).^{50,55} Maximum uptakes at $p/p_0 \sim 0.029$ were between 0.06 and 0.12 mmol g⁻¹ for shales and between 0.27 and 0.74 mmol g⁻¹ for kerogens (Table S3). Thus, CO₂ uptake on kerogen is about 5 times higher than on shales under these conditions.

The Dubinin-Radushkevich (DR) model was used to calculate ultramicropore volumes using a density of 1.032 g cm⁻³ (liquid density of CO₂ at -20°C).⁵⁶ A value of 1.023 g cm⁻³ was used previously in a detailed study of the adsorption of CO₂ on activated carbons.⁵⁰ Additionally, a non-local density functional theory (NLDFT) equilibrium model with a kernel based on slit-shaped pores in carbon was used to calculate pore size distributions (see Supporting Information, Section G, Figures S7 and S8) and micropore volumes from the isotherms. These pore size distributions (< 5 nm) are shifted to slightly lower pore sizes compared with Eagle Ford shale obtained from nitrogen (-196°C).⁵⁷ Table 4 shows that the ultramicropore volumes in shales, estimated from the DR model range from 4.6 to 8.0 mm³ g⁻¹, or from 4.0 to 7.7 mm³ g⁻¹ estimated from the NLDFT model. Ultramicropores thus represent approximately 12% of total pore volume in Wickensen and Hadessen samples, and 25 and 41% of total pore volume in the Harderode samples. Ultramicropore volumes follow the same trends as CO₂ sorption pore volumes. There is only a weak trend of micropore volume with maturity for the shales.

Ultramicropore volumes in kerogens are much higher than in shales, ranging from 27.0 to 54.6 mm³ g⁻¹, estimated from the DR model, and 21.8 to 50.8 mm³ g⁻¹ according to the NLDFT model (see Table 4). Ultramicropore volumes are similar in Wickensen ($R_0 = 0.53\%$) and Harderode ($R_0 = 0.89\%$) samples, but are almost double in the Hadessen ($R_0 = 1.45\%$) samples (see Table 4).

1
2
3 Even though the models are entirely different, NDLFT micropore volumes generally
4 agree well with the DR ultramicropore volumes. NDLFT micropore size distributions are
5 shown in Supporting Information (Figures S7 and S8). The pore size distribution show very
6 little porosity above a pore width of about 1 nm, confirming that CO₂ at 0°C and 0.1 MPa is
7 limited to ultramicroporosity.
8
9

10
11
12 DR micropore volumes were also calculated from nitrogen -196°C isotherms. At low
13 relative pressure nitrogen fills micropores < 2 nm providing there is no activated diffusion or
14 molecular sieving. The N₂ micropore volumes are shown in Table 4. For kerogen the N₂
15 micropore volumes are significantly lower than the CO₂ ultra-micropore volume probably
16 reflecting some activated diffusion or molecular sieving, as mentioned in section 3.2.2
17 However, the nitrogen micropore volumes increase with increasing maturity in a similar
18 manner to the CO₂ ultramicropore volumes. This large increase in micropore volume might
19 be due to the generation of slightly larger micropores in kerogen through which nitrogen
20 can diffuse more readily.
21
22
23
24
25
26
27
28

29 **3.3 Methane Sorption**

30 **3.3.1 Shale**

31
32 Shale isotherms were measured at 45, 65 and 85°C and up to ~14 MPa. Excess shale
33 isotherms are show in Figures 6 and 7. Tabulated isotherm data are given in Supporting
34 Information Table S6. Isotherms at 45°C for HAR7060 and HAD7090 show a distinct excess
35 maximum, while the other isotherms show plateaus. Maximum surface excess uptakes are
36 between 0.096 and 0.119 mmol g⁻¹ for Wickensen and Hadessen shales while uptake on
37 Harderode shales were lower, with maxima of 0.054 and 0.070 mmol g⁻¹(Table S6).
38 Maximum methane surface excess uptake decreases with increasing temperature for all
39 shales. Furthermore, at 65°C and 85°C the isotherms do not have a distinct maximum in the
40 pressure range used in this study.
41
42
43
44
45
46
47
48
49

50 **3.3.2 Kerogen**

51
52 Kerogen isotherms were measured at 45 and 65°C and up to ~14 MPa. The surface
53 excess isotherms are shown in Figures 8 and 9 and tabulated data are given in Table S6. The
54 pressure range is not large enough for the isotherms to reach the excess maximum or
55 plateau. WIC and HAR kerogens take up between 0.45 - 0.58 mmol g⁻¹ at ~13.5 MPa and
56
57
58
59
60

1
2
3 45°C, which is similar to Pennsylvanian coals of various rank ($V_R = 0.72 - 1.56\%$).⁵⁸ Maximum
4 uptake on HAD kerogens ($R_0 = 1.45\%$) was higher (0.90 - 0.95 mmol g⁻¹ at 45°C and ~14 MPa)
5 than on WIC ($R_0 = 0.53\%$) and HAR ($R_0 = 0.89\%$) kerogens. This shows the increase in
6 adsorption capacity at the onset of the gas window.
7
8
9

10 11 **3.3.3 Methane Sorption and Pore Volumes**

12
13 There is only a weak correlation ($R^2=0.48$) of maximum excess uptake at 45°C on
14 shale and TOC (see Figure 10). However, there is a very strong correlation of methane
15 uptake and CO₂ sorption pore volume. Figure 11 shows methane uptake on shale and
16 kerogen at 45°C and 10.0 MPa against the CO₂ sorption pore volume, with a regression line
17 which goes through the origin. A strong correlation also exists between methane uptake at
18 65°C and 11.5 MPa and CO₂ sorption pore volume (see Figure 12). Similar correlations are
19 obtained at lower pressures (see Figures S9a and b) and also at 85°C (see Figure S9c). The
20 correlations suggest that supercritical methane sorption on Posidonia shales and kerogens
21 takes mainly place in pore volumes as measured by CO₂ sorption at -78°C. Both the CO₂
22 subcritical and methane supercritical adsorption studies show that kerogens have much
23 larger adsorption than for the corresponding shales (see Figures 11 and 12). Comparison of
24 kerogen and shale isotherms with TOC measurements indicate that the shale adsorption
25 exceeds that which can be accounted for by the kerogen alone, indicating that significant
26 adsorption occurs in the inorganic phase of the shale. The Sorption mass balances for
27 kerogens and inorganic phase materials (clays etc.) are discussed later.
28
29
30
31
32
33
34
35
36
37
38
39
40

41 **3.3.4 Absolute isotherms and parameterization**

42
43 The absolute isotherm can be calculated from the excess isotherm using the
44 following equation
45
46

$$47 \quad n_{ab} = n_{ex} + \rho_b * V_{ad} \quad (1)$$

48
49
50
51
52
53 Where n_{ex} is the excess amount adsorbed, ρ_b is bulk gas phase density and V_{ad} is the
54 adsorption pore volume. Equation (1) has been used for crystalline zeolites and metal
55 organic frameworks, where the structure can be determined from X-ray or neutron
56
57
58
59
60

1
2
3 diffraction studies. Good agreement has been observed between crystallographic data and
4 pore volumes measured by gas adsorption for microporous metal organic framework
5 materials.^{59,60} In these materials, V_{ad} is assumed to be equal to the crystallographic pore
6 volume, which is an inherent property of the adsorbent.^{61,62} However, for heterogeneous
7 materials, such as shales, which have a wide pore size distribution, this is more problematic
8 since adsorption in the larger pores may not be significant.⁶³ In the shales used in this study,
9 the subcritical CO₂ sorption pore volumes were 21-32% of the total pore volume for the WIC
10 and HAD shale samples and 46-66% of the total pore volume for the HAR shale samples (see
11 Table 4). It is evident that in these materials, V_{ad} is significantly lower than the total pore
12 volume. It is important to distinguish between the adsorbed and bulk gas phases in shale in
13 order to understand the occurrence of adsorbed gas in shale and therefore, V_{ad} needs to be
14 estimated. Studies of a high maturity Alum shale showed that subcritical pore volumes
15 obtained from adsorption of CO₂ (-78°C and 0°C), N₂ (-196°C) and CH₄ (-161°C) agreed within
16 ± 5%.¹¹ Hence, the CO₂ sorption pore volume at -78°C is a reasonable estimate for an upper
17 limit for V_{ad} . Therefore, in this study, a sorption volume balance for the shales was
18 investigated by measuring the total pore volume (< 1093 nm) from helium pycnometry,
19 grain density and mercury bulk density; mercury injection capillary pressure porosimetry
20 and gas sorption pore volumes.
21
22
23
24
25
26
27
28
29
30
31
32
33
34

35 The Washburn equation indicates that mercury enters pores with constrictions with
36 equivalent diameters > 1093 nm at 1.379 MPa. Therefore, at 1.379 MPa, $1/\rho_{HgBulk}$ will be
37 equal to the volume of the shale and pores < 1093 nm, where ρ_{HgBulk} is the mercury bulk
38 density of the shale. Assuming helium enters all accessible pores and is not adsorbed; $1/\rho_{He}$
39 is equal to the volume of shale, where ρ_{He} is the density of the shale measured by helium
40 pycnometry. Therefore, the total pore volume (< 1093 nm) is given by the following
41 equation.
42
43
44
45
46
47

$$48 \quad \text{Total Pore Volume (< 1093 nm)} = \frac{1}{\rho_{HgBulk}} - \frac{1}{\rho_{He}} \quad (2)$$

49 and the Total Porosity (< 1093 nm)

$$50 \quad \text{Total Porosity (< 1093 nm)} = 1 - \frac{\rho_{HgBulk}}{\rho_{He}} \quad (3)$$

1
2
3 Alternatively, since the helium and grain densities are similar within experimental error, ρ_{He}
4 can be replaced by ρ_{Grain} in equations (2) and (3).
5
6

7
8 Figure 3 shows that a graph of Total Pore Volume (< 1093 nm) versus CO₂ sorption
9 pore volume (CO_2SPV) + mercury injection pore volume ($MICP_{PV}$) corresponding to equation
10 (4) below, has good linearity ($R^2 = 0.974$) for the 6 shales studied, which vary markedly in
11 maturity.
12
13

$$14 \quad Total \ Pore \ Volume(< \ 1093 \ nm) = \ CO_2 \ SPV + \ MICP_{PV} \quad (4)$$

15
16
17 The $MICP_{PV}$ corresponds to the difference between the mercury injected at 1.379 and 268.9
18 MPa, and $CO_2 \ SPV$ is the pore volume obtained from CO₂ adsorption at 0.1 MPa and -78°C
19 using a CO₂ adsorbed phase density of 1.177 g cm⁻³. The $CO_2 \ SPV$ characterizes the
20 microporosity and some mesoporosity where gas adsorption predominates, while the
21 $MICP_{PV}$ characterizes the mesoporosity > 5.6 nm and macroporosity up to 1093 nm. The
22 upper size limit for significant CO₂ adsorption is unknown, but the linear relationship in
23 Figure 3 indicates that it is approximately 5-6 nm. However, there will be very small
24 amounts of adsorption in larger pores. The linearity of the relationship indicates that all the
25 accessible porosity < 1093 nm has been taken into account by the combination of CO₂
26 sorption and mercury injection. It is not possible to use mercury injection porosimetry for
27 isolated kerogens. The strong linear ($R^2 = 0.9557$ and 0.9727) correlation between CH₄
28 sorption uptake and CO₂ sorption pore volume for both shales and kerogens used in this
29 study suggest that supercritical methane sorption in shales and kerogen takes place in the
30 CO₂ sorption pore volume (see Figures 11 and 12). These correlations support the use of
31 the CO₂ sorption pore volume (-78°C) for V_{ad} to estimate absolute isotherms and thus,
32 quantify the sorbed phases in shales. Also, it provides an estimate of adsorbed phase versus
33 bulk "free" gas phase contributions to methane stored in shale.
34
35
36
37
38
39
40
41
42
43
44
45
46
47
48

49 The absolute isotherms of shales and kerogen are shown in Figure 13 and Figure 14.
50 Absolute amounts on HAD shales at ~13 MPa and 85°C are 0.14 and 0.18 mmol g⁻¹. HAD
51 kerogens exhibit much higher absolute amounts adsorbed of 1.21 and 1.31 mmol g⁻¹ (at 13
52 MPa and 65°C). Mass balance calculations between the shale and kerogen data obtained by
53 normalizing these uptakes with TOC and comparison with the uptake on shale under the
54
55
56
57
58
59
60

1
2
3 same conditions, shows that approximately 50% of the methane uptake in HAD shales is
4 within the kerogen.
5

6
7 The Dubinin-Radushkevich and Langmuir equations can be used as semi-empirical
8 equations to parameterize the methane absolute isotherms. The supercritical Dubinin-
9 Radushkevich equation has been shown to describe methane isotherms more accurately
10 than the Langmuir equation over a wide temperature range (27-200 °C) for an Alum shale
11 sample.¹¹ The DR micropore volume was 77 % of the CO₂ sorption pore volume in the Alum
12 shale and this is significantly higher than the shales used in this study, which were in the
13 range 40-62%. However, the Posidonia Shale and kerogen absolute and excess isotherms for
14 45, 65 and 85°C were described more accurately by a modified version of the Langmuir
15 equation:
16
17
18
19
20
21
22

$$n_{ab} = n_{ab,max} \frac{K(T) f}{1+K(T) f} \quad (5)$$

23
24
25
26
27 where $n_{ab,max}$ is the maximum absolute amount adsorbed, $K(T)$ is the Langmuir parameter, f
28 is fugacity. One fitting parameter can be eliminated by using $n_{ab,max} = CO_2SPV * \rho_{ad,max}$ where
29 CO_2SPV is the CO₂ sorption pore volume and $\rho_{ad,max}$ is the maximum adsorbed phase density.
30 The shale and kerogen absolute and excess isotherms were fitted to Equation (5) with 2
31 fitting parameters for shales and kerogens, the temperature-dependent Langmuir
32 parameter $K(T)$ and the maximum adsorbed phase density ($\rho_{ad,max}$). Due to the narrow
33 temperature range (45-85°C for shale and 45-65°C for kerogen) $\rho_{ad,max}$ was assumed to be
34 independent of temperature. Other studies on shale sorption have used pressure instead of
35 fugacity in the Langmuir model.^{12,16} The use of pressure instead of fugacity gave almost
36 identical results to those presented in Table 4.
37
38
39
40
41
42
43
44
45

46 Good fits were obtained for shale and kerogen isotherms. The calculated parameters
47 are shown in Table 5 and the fits of the model to the absolute isotherms at 65°C are shown
48 in Figure 13 for shale and Figure 14 for kerogen. The corresponding CH₄ adsorption data at
49 45°C and 85°C are given in Supporting Information, Figures S4-S6. The adsorbed phase
50 densities of methane on shale are all below the liquid density of methane (425.1 kg m⁻³ at
51 boiling point: -161.49°C and 101.3 kPa).⁵⁶ The hypothesis is that adsorbed phase densities in
52 the pores do not exceed the liquid density of the sorptive. The adsorbed phase densities of
53
54
55
56
57
58
59
60

1
2
3 WIC and HAR shales are within 11% of the methane adsorbed phase density on shale
4 determined by molecular simulations (370 kg m^{-3}) by Ambrose et al.⁶⁴ The adsorbed phase
5 densities of HAD shales ($\sim 290 \text{ kg m}^{-3}$) are lower. This could be due to wider pores in the
6 HAD gas window shales ($R_0 = 1.45\%$), as indicated earlier. The Langmuir constants and
7 adsorbed phase densities are similar to the values determined by Gasparik et al. on Aalborg
8 and Sleen shale samples at 65°C ($K(65) = 0.064 - 0.104 \text{ MPa}^{-1}$; $295 - 332 \text{ kg m}^{-3}$).¹⁶ The
9 calculated adsorbed phase densities for all kerogens with the exception of HAD7090 are
10 above the liquid methane density suggesting that the Langmuir model may have significant
11 limitations for determining physically reasonable sorption parameters or possibly, there are
12 sorption induced volumetric changes.
13
14
15
16
17
18
19
20

21 **3.3.5 Distribution of high-pressure methane sorption**

22
23
24 Mass balances of methane sorption on shales were determined to investigate the
25 distribution of sorption sites between kerogen plus clay minerals and the organic-inorganic
26 interface. Methane sorption on clay minerals has been studied previously.^{65,66} Ji et al.⁶⁵ have
27 measured methane sorption at 65°C up to around 10 MPa on montmorillonite, kaolinite,
28 chlorite and illite at 65°C while Liu et al.⁶⁶ measured methane sorption on montmorillonite,
29 kaolinite and illite at 60°C and up to 18 MPa. The clay sorption data and kerogen sorption
30 data were normalized by the XRD data and TOC, respectively, and compared against shale
31 isotherm at 65°C . Results are shown in Figure 15. Around 45 – 60% and 60 – 70% of the
32 methane sorption can be attributed to clays and kerogen in WIC and HAD shales,
33 respectively, whereas kerogen and clay minerals can account for the entire sorption
34 capacity measured on HAR shales.
35
36
37
38
39
40
41
42
43

44 **3.3.6 Enthalpy of Adsorption of shales**

45
46
47 The isosteric enthalpies of adsorption can be calculated for a pure gas using the equation
48 below.⁶⁷
49

$$50 \quad Q_{st,n} = RT^2 \left[\frac{\delta \ln P}{\delta T} \right]_n \quad (6)$$

51
52
53
54
55 Where $Q_{st,n}$ is the isosteric enthalpy of adsorption at a surface excess loading n , P is pressure,
56 T is temperature and R is the gas constant. The surface excess is approximately equal to the
57
58
59
60

absolute amount adsorbed at low pressure. The isosteric enthalpy of adsorption at zero surface coverage ($Q_{st,n=0}$) is a fundamental measure of the adsorbate interaction with the adsorbent. At the zero surface coverage adsorption limit, the isosteric enthalpies of adsorption derived from surface excess and absolute isotherms should be identical.

The methane absolute isotherms were calculated using equation (1) and the CO₂ sorption pore volume (-78°C). The isosteric enthalpies of adsorption of methane on shale and kerogen were calculated at zero surface coverage by two methods (Myers and Monson⁶⁸ and virial equation^{69,70}). The virial equation at low surface coverage is given below:

$$\ln\left(\frac{n_{ab}}{p}\right) = A_0 + A_1 n_{ab} \quad (7)$$

where n_{ab} is the absolute amount adsorbed (mmol g⁻¹), p is pressure (Pa), A_0 and A_1 are virial parameters. The slope of the graph of A_0 against T^{-1} gives ($Q_{st,n=0}/R$). The Henry's Law constant is given by the equation below:

$$K_H = \exp(A_0) \quad (8)$$

The $Q_{st,n=0}$ was also determined using the Langmuir equation (5), which provide a good fit for the experimental data. Myers and Monson define the absolute uptake as the amount of gas inside the pore volume and use the Langmuir equation to derive Q_{st} .⁶⁸ In the case of shales, which have a significant amount of meso- and macroporosity, the sorption pore volume is the volume of increased density due to sorption. The equation derived is:

$$C = \frac{1}{P^0} \exp\left(\frac{A}{R}\right) \exp\left(\frac{-B}{RT}\right) \quad (9)$$

Where C is the constant in the Langmuir equation, which is a function of temperature; B is the enthalpy of adsorption (kJ mol⁻¹), and $P^0 = 1$ bar is the pressure at the perfect-gas reference state. The temperature-independent component $\exp(A/R)$ is an entropic factor.

The enthalpies of CH₄ adsorption at zero surface coverage on shales and kerogens calculated by both methods are shown in Table 6. The enthalpies of adsorption for shales and kerogen are very similar for calculations by both methods. The average values for $Q_{st,n=0}$ for shale are 14.4 ± 1.6 kJ mol⁻¹ (Virial Method⁶⁹) 12.2 ± 1.0 kJ mol⁻¹ (Myers and Monson Method⁶⁸) while the values for kerogens are 13.1 ± 1.9 kJ mol⁻¹ (Virial Method⁶⁹) and 13.4 ± 3.0 kJ mol⁻¹ (Myers and Monson Method⁶⁸). No clear trend with maturity was observed. The

1
2
3 $Q_{st,n=0}$ values are slightly lower than the corresponding enthalpy of $19.2 \pm 0.1 \text{ kJ mol}^{-1}$
4 determined at $0.025 \text{ mmol g}^{-1}$ for an Alum shale, which had a greater proportion of
5 ultramicroporosity. Similar results have been obtained for a Barnett shale from the gas
6 window ($R_0 = 2.01\%$, $Q_{st} = 18.4 \text{ kJ mol}^{-1}$).¹² Shales from the pre-gas window had lower
7 isosteric enthalpies of adsorption ($Q_{st} = 7.3 - 15.3 \text{ kJ mol}^{-1}$).¹² The range of isosteric
8 enthalpies obtained for CH_4 adsorption on other porous materials are similar (activated
9 carbon ($Q_{st} = 9-20 \text{ kJ mol}^{-1}$)⁷¹⁻⁷³ and coal ($Q_{st} = 10-22 \text{ kJ mol}^{-1}$)^{74,75}). It is apparent that the
10 strength of interactions of methane with porosity in various shales are similar and also,
11 similar to CH_4 adsorption on carbonaceous materials. There are, at most, small differences
12 in adsorption enthalpy with maturity or uptake for the samples studied. The
13 thermodynamics discussed above and the correlation of supercritical CH_4 adsorption uptake
14 with CO_2 sorption pore volume (-78°C) for shales suggest that the amount adsorbed is
15 controlled by the available porosity ($< \sim 6 \text{ nm}$) rather than the strength of the interaction of
16 CH_4 with the pore walls in shales.
17
18
19
20
21
22
23
24
25
26
27
28
29

30 4 DISCUSSION

31 Comparison of the subcritical CO_2 isotherms for Posidonia shales and the
32 corresponding kerogen isotherms shows that they have similar shapes. Both the DR
33 micropore volumes (CO_2 , 0°C) and sorption pore volumes (CO_2 , -78°C) increase with
34 increasing total pore volumes and have approximately linear trends for the shales (see
35 Figures S11 a, b and c). The DR micropore volumes (CO_2 , 0°C) and sorption pore volumes
36 (CO_2 , -78°C) has a similar trend for the kerogens and better linearity ($R^2 = 0.8893$) (see
37 Figures S11 d). However, no specific trends are expected between these parameters. The
38 DR micropore volumes (CO_2 , 0°C) and sorption pore volumes (CO_2 , -78°C) for the kerogens
39 are 3.6-9.1 and 4.6-10.5 times larger than the corresponding shales indicating the potential
40 importance of the kerogen in determining CH_4 storage capacity. Comparison of the DR
41 micropore volumes (CO_2 , 0°C) and sorption pore volumes (CO_2 , -78°C) for shales and
42 kerogens shows no correlation suggesting that adsorption in the inorganic phase (clays etc.)
43 makes a significant contribution to subcritical adsorption (see Figures S11e and f).
44 Comparison of the supercritical high pressure methane isotherms for the Posidonia
45 kerogens and shales shows that similar trends to the CO_2 subcritical isotherms are observed,
46 with the kerogen uptakes being $\sim 3.6 - 8.4$ times greater than the corresponding shale at
47
48
49
50
51
52
53
54
55
56
57
58
59
60

1
2
3 11.5 MPa and 65°C. However, the TOC values for the samples studied are in the range 5.78 -
4 10.92%, and therefore, the inorganic phase is >89% of the shales. The sorption mass balance
5 between kerogen and shale indicates that methane storage in the inorganic phase of dry
6 shales is also significant.
7
8
9

10
11 Posidonia kerogens have DR micropore volumes which are at the lower end of the
12 range of micropore volumes measured on various coals (0.014 – 0.057 cm³ g⁻¹).⁷⁶⁻⁷⁸ A trend
13 of DR micropore volume with maturity for coals has been reported with DR micropore
14 volume decreasing from high volatile to medium volatile bituminous coals and then
15 increasing with further coalification.^{45,76,79} The decrease in micropore volumes was
16 attributed to the filling of pores by low-volatile hydrocarbons and the subsequent increase
17 to the cracking of the occluded oils with coalification.^{45,79} Similar trends were observed in
18 DR micropore and sorption pore volumes in this study, suggesting that there is pore
19 generation and/or pore opening by cracking of occluded oil in gas-window Posidonia
20 kerogens. Micropore 'blocking' by bitumen in the oil-window kerogens (HAR) may take
21 place, similar to coal. The presence of low-volatile bitumen is suggested by the relatively low
22 helium densities of HAR kerogens compared with HAD kerogens, which had the highest
23 densities (see Table 1). The shale CO₂ DR micropore and sorption pore volumes reach a
24 minimum in the oil window. However, kerogens do not show a well-defined minimum in the
25 oil window. There is no significant change from WIC to HAR, but an increase to HAD. It is
26 apparent that changes in the microporosity of kerogen are probably controlling changes in
27 the microporosity of shales into the gas-window.
28
29
30
31
32
33
34
35
36
37
38
39
40

41 The shale pore volume is comprised of contributions from inorganic materials (including
42 phyllosilicates, etc), kerogens and the interface region between these materials. The
43 contribution of the kerogen component to the shale porosity can be determined by
44 normalizing the kerogen pore volume with TOC. This shows that approximately half of the
45 CO₂ sorption pore volume for a given shale is within the organic matter for all Posidonia
46 shale samples. The other part of the porosity cannot be attributed to any specific mineral
47 type as comparisons of mineral composition with pore volumes do not show any
48 correlations. However, previous publications have concluded that micropores are present in
49 clay but not in quartz,¹⁴ although the clay content variation in Posidonia shales
50 (illite/smectite ranging from only 18.5 – 26.2 wt%, kaolinite 1.1 – 8.9 wt%) is too small to
51
52
53
54
55
56
57
58
59
60

1
2
3 show any trend with pore volume. The role of clays for sorption in dry shales is consistent
4 with the similar shapes of kerogen and clay mineral isotherms.¹⁴
5
6

7
8 Since the sum of porosity measured by (a) CO₂ adsorption at -78°C and (b) mercury
9 injection is very similar to total porosity, and since mercury injection measures pore
10 constrictions larger than approximately ~6 nm, we infer that most of the CO₂ sorption
11 porosity is in pores smaller than ~6 nm. The very strong correlation between CH₄ maximum
12 excess uptake and CO₂ sorption volume suggests that most CH₄ is sorbed in pores, which are
13 smaller than ~ 6 nm and associated with both kerogen and clay minerals. Grand canonical
14 Monte Carlo simulations of methane adsorption have been carried out for graphitic surfaces,
15 as models for kerogens, across a range of pore sizes for various temperature and pressure
16 conditions. The results suggest that adsorbed methane density changes non-monotonically
17 with increasing pore width, and decreases to a minimum in 1.2 nm pores at 12 MPa.⁸⁰ Cai
18 et al⁸¹ suggested that the pore volume, with pore widths in the range 2 – 5 nm, was the
19 primary control for methane adsorption capacity of coals from Northeastern China.
20
21
22
23
24
25
26
27
28

29
30 Methane isotherms for shales and kerogens normalized to TOC are shown in Figure
31 S10a-f. It is apparent that the TOC normalized isotherms for shales are always higher than
32 the corresponding kerogen isotherms. This indicates significant methane adsorption in the
33 inorganic component of the shale. A mass balance for CH₄ sorption based on the kerogen
34 isotherms measured in this study and the illite or smectite isotherms published by Ji et al⁶⁵
35 and Liu et al⁶⁶ suggests that for HAR shales, all the CH₄ sorption can be accounted for by
36 uptake on clay minerals and kerogen. However, only 45-60% of the sorption of WIC shales
37 and 60-70% of the sorption of HAD shales can be accounted for by a mass balance of
38 sorption by kerogen and clay minerals (Figure 15).^{65,66} Sorption mass balances determined
39 using kerogen and shale isotherms suggest that in dry natural shales, possibly significant
40 sorption also occurs at interfaces between kerogen and clay minerals for the WIC and HAD
41 shales. Also, the kerogen separation process may modify its adsorption characteristics, and
42 some other inorganic materials not accounted for in the sorption mass balance may
43 increase sorption.
44
45
46
47
48
49
50
51
52
53
54

55 We note that since water is present in natural subsurface shales, pores associated
56 with clay minerals may be at least partly water-filled, in which case they will not contribute
57
58
59
60

1
2
3 to the sorption pore volume. The adsorbed phase in porous systems is in equilibrium with
4 the homogeneous bulk gas phase in meso- and macropores. Fracturing shale and releasing
5 gas from the bulk gas phase allows the sorbed gas to desorb. The amount of gas released
6 (sorbed + bulk gas) at reservoir temperatures can be estimated from the excess isotherms
7 and total pore volumes. The amount of gas desorbed can be visualized directly from the
8 absolute isotherms. Absolute CH₄ sorption on dry Posidonia shales at 65°C and 15 MPa
9 ranges from 0.092 - 0.202 mmol g⁻¹ (66 – 144 scf t⁻¹) on dry shale, and from 0.76 - 1.32 mmol
10 g⁻¹ (540 – 942 scf t⁻¹) on dry kerogen. Absolute amounts adsorbed at 85°C and 15 MPa are
11 103 and 127 scf ton⁻¹ in dry Hadessen shales. The shapes of the absolute shale and kerogen
12 isotherms indicate that only small amounts of gas will desorb at high pressure. This is not
13 only because most sorbed gas is within pores smaller than approximately 6 nm, but also,
14 comparison of the DR micropore volumes obtained from CO₂ adsorption at 0°C suggests
15 that 40 – 62 % of the sorption pore volumes in shales and 39 – 53 % in kerogen are
16 ultramicroporous. Gas in ultramicropores is strongly sorbed due to the proximity of the
17 walls and the resulting high sorption potential. Furthermore, there is no significant variation
18 of enthalpies of adsorption determined from high-pressure methane isotherms, indicating
19 that the interactions of the pore surfaces and the methane molecules are similar in all these
20 Posidonia samples and is not affected by maturity.

21
22
23
24
25
26
27
28
29
30
31
32
33
34
35
36 Although N₂ isotherms at -196°C are often used to characterize porosity they can be
37 misleading.⁸² The narrowest ultramicroporosity cannot be accessed by nitrogen molecules
38 at -196°C, due to activated diffusion. Furthermore, microporous solids may give rise to
39 unrealistically high BET surface areas as micropore filling may occur. Both issues have been
40 pointed out on coal previously.⁸³

41
42
43
44
45
46 While the supercritical Dubinin-Radushkevich equation produced good fits for CH₄
47 sorption in a previous study on Alum shale, Posidonia shale are more accurately described
48 by the Langmuir equation.⁸ In comparison to the Posidonia shales, the Alum shale has a
49 larger proportion of ultra-microporosity (DR CO₂ ultramicropore volume of 12.9 and CO₂
50 sorption pore volume of 16.8 mm³ g⁻¹).¹⁴ The DR model is based on micropore filling and,
51 thus, it produced good results on ultra microporous shales. The Posidonia shales have a
52 much greater fraction of larger pores as shown by the ratio of the CO₂ -78°C sorption pore
53 volume to the CO₂ (0°C) DR micropore volume (see Table 4) and this may be the reason for
54
55
56
57
58
59
60

1
2
3 the Langmuir model providing a better fit than the DR equation for the Posidonia isotherm
4 data.
5
6
7

8 **5 CONCLUSIONS**

9
10 Methane sorption capacities and pore characteristics of bulk shales and isolated
11 kerogens have been determined for immature, oil-window and gas-window samples from
12 the Lower Toarcian Posidonia Shale formation. Total porosities and CO₂ sorption volumes (-
13 78°C) of organic-rich Posidonia shales decrease through the oil-window and then increase
14 into the gas-window. This implies that part of the sorption porosity is blocked by bitumen
15 and then regenerated as a result of gas generation from bitumen and/or kerogen. Since (a)
16 the sum of porosities measured by CO₂ at -78°C and mercury injection are very similar to the
17 corresponding total pore volume (< 1093 nm) thereby accounting for all the available shale
18 porosity and (b) mercury at 268.9 MPa occupies pores with constrictions larger than ca. 6
19 nm, we infer that porosity measured by CO₂ adsorption at -78°C is largely within pores
20 smaller than 6 nm. The CO₂ sorption pore volume represents 21 to 66 % of the total pore
21 volume in these shales, with 10 to 41 % of the total pore volume in DR micropore pore
22 (<~0.7 nm) volume. Porosity information from subcritical nitrogen sorption at -196°C is not
23 applicable due to activated diffusion effects.
24
25
26
27
28
29
30
31
32
33
34
35

36 A modified Langmuir model including the sorption pore volume fits the absolute and
37 surface excess CH₄ isotherms well and this provides a useful parameterization of the data.
38 Methane is sorbed strongly in ultramicropores and will only be desorbed at low pressure.
39 Enthalpies of methane adsorption on dry shales range from 11.2 - 15.7 kJ mol⁻¹ and from 8.5
40 - 17.2 kJ mol⁻¹ on kerogen, and are not related to maturity. The linear correlation between
41 maximum CH₄ sorption and CO₂ sorption pore volume (-78°C) is very strong for both shales
42 and kerogens, and suggests that the vast majority of sorbed CH₄ occurs in pores smaller
43 than 6 nm, with around half of that within ultramicroporosity in the shales studied. Shale
44 and kerogen mass balance considerations indicate that approximately half of the CH₄
45 sorption on dry shales takes place within the organic matter and this indicates the
46 significance of the inorganic phase, including the role of clays and possibly the organic-
47 inorganic interface as sorption sites in dry shales. However, caution is required in
48 extrapolating these results to the subsurface, where water may occur.
49
50
51
52
53
54
55
56
57
58
59
60

1
2
3
4
5
6
7
8
9
10
11
12
13
14
15
16
17
18
19
20
21
22
23
24
25
26
27
28
29
30
31
32
33
34
35
36
37
38
39
40
41
42
43
44
45
46
47
48
49
50
51
52
53
54
55
56
57
58
59
60

1
2
3 **ACKNOWLEDGMENTS**
4

5
6 This work was supported by the Wolfson Foundation and the GASH project funded by
7
8 Bayerngas, ExxonMobil, GdFSuez, Marathon, Repsol, Schlumberger, Statoil, Total, Vermilion
9
10 and Wintershall.

11
12 **ASSOCIATED CONTENT**
13

14 Supporting Information available includes tabulated supercritical methane and subcritical
15 carbon dioxide and nitrogen adsorption isotherm data (Tables S3-S6), micropore size
16 distributions (Figures S7 and S8), Langmuir parameterization data (Figures S4-S6),
17 comparisons of various characterization parameters (Figures S9 and S11), instrument
18 parameters (Table S2) and associated text. Kerogen isolation, verification of purity by X-ray
19 diffraction (Figure S1), kerogen pyrite content (Table S1), pyrite adsorption isotherm (Figure
20 S2) are also included. Shale and kerogen isotherms normalized to TOC are compared in
21 Figure S10
22
23
24
25

26 This material is available free of charge via the Internet at <http://pubs.acs.org>.
27

28
29 **AUTHOR INFORMATION**
30

31 **Corresponding Author**
32

33 E-mail: mark.thomas@ncl.ac.uk
34

35
36 **Notes**
37

38 The authors declare no competing financial interest.
39
40
41
42
43
44
45
46
47
48
49
50
51
52
53
54
55
56
57
58
59
60

■ REFERENCES

- (1) EIA, U. S. *Annual Energy Outlook 2013*, 2013.
- (2) Borst, R. L. *Sedimentology* **1982**, 29, 291.
- (3) Yang, Y. L.; Aplin, A. C. *Mar. Pet. Geol.* **1998**, 15, 163.
- (4) Cartwright, J. A.; Dewhurst, D. N. *Geological Society of America Bulletin* **1998**, 110, 1242.
- (5) Loucks, R. G.; Reed, R. M.; Ruppel, S. C.; Jarvie, D. M. *J. Sediment. Res.* **2009**, 79, 848.
- (6) Loucks, R. G.; Reed, R. M.; Ruppel, S. C.; Hammes, U. *AAPG Bull.* **2012**, 96, 1071.
- (7) Milliken, K. L.; Rudnicki, M.; Awwiller, D. N.; Zhang, T. W. *AAPG Bull.* **2013**, 97, 177.
- (8) Clarkson, C. R.; Freeman, M.; He, L.; Agamalian, M.; Melnichenko, Y. B.; Mastalerz, M.; Bustin, R. M.; Radliński, A. P.; Blach, T. P. *Fuel* **2012**, 95, 371.
- (9) Mastalerz, M.; He, L.; Melnichenko, Y. B.; Rupp, J. A. *Energy Fuels* **2012**, 26, 5109.
- (10) Ruppert, L. F.; Sakurovs, R.; Blach, T. P.; He, L.; Melnichenko, Y. B.; Mildner, D. F. R.; Alcantar-Lopez, L. *Energy Fuels* **2013**, 27, 772.
- (11) Rexer, T. F. T.; Benham, M. J.; Aplin, A. C.; Thomas, K. M. *Energy Fuels* **2013**, 27, 3099.
- (12) Zhang, T. W.; Ellis, G. S.; Ruppel, S. C.; Milliken, K.; Yang, R. S. *Org. Geochem.* **2012**, 47, 120.
- (13) Gasparik M.; Bertier P.; Gensterblum Y.; Ghanizadeh A.; Krooss B. M.; Littke R. *Int J Coal Geology* **2014**, 123, 34.
- (14) Ross, D. J. K.; Bustin, R. M. *Mar. Pet. Geol.* **2009**, 26, 916.
- (15) Weniger, P.; Kalkreuth, W.; Busch, A.; Krooss, B. M. *Int. J. Coal Geol.* **2010**, 84, 190.
- (16) Gasparik, M.; Ghanizadeh, A.; Bertier, P.; Gensterblum, Y.; Bouw, S.; Krooss, B. M. *Energy Fuels* **2012**, 26, 4995.
- (17) Chareonsuppanimit, P.; Mohammad, S. A.; Robinson, R. L.; Gasem, K. A. M. *Int. J. Coal Geol.* **2012**, 95, 34.
- (18) Lu, X. C.; Li, F. C.; Watson, A. T. *Fuel* **1995**, 74, 599.
- (19) Chalmers, G. R. L.; Bustin, R. M. *Bull. Can. Pet. Geol.* **2008**, 56, 22.
- (20) Chalmers, G. R. L.; Bustin, R. M. *Int. J. Coal Geol.* **2007**, 70, 223.
- (21) Littke, R.; Baker, D. R.; Leythaeuser, D. *Org. Geochem.* **1988**, 13, 549.
- (22) Vandenbroucke, M.; Behar, F.; Santorcuato, A.; Rullkotter, J. *Org. Geochem.* **1993**, 20, 961.
- (23) Vandenbroucke, M.; Largeau, C. *Org. Geochem.* **2007**, 38, 719.

1
2
3 (24) Rullkotter, J.; Leythaeuser, D.; Horsfield, B.; Littke, R.; Mann, U.;
4 Muller, P. J.; Radke, M.; Schaefer, R. G.; Schenk, H. J.; Schwochau, K.; Witte, E.
5 G.; Welte, D. H. *Org. Geochem.* **1988**, *13*, 847.

6
7 (25) Littke, R.; Baker, D. R.; Leythaeuser, D.; Rullkotter, J. *KEYS TO*
8 *THE DEPOSITIONAL HISTORY OF THE POSIDONIA SHALE (TOARCIAN) IN*
9 *THE HILS SYNCLINE, NORTHERN GERMANY*; Geological Soc Publishing
10 House: Bath, 1991.

11 (26) Bernard, S.; Horsfield, B.; Schulz, H.-M.; Wirth, R.; Schreiber, A.;
12 Sherwood, N. *Mar. Pet. Geol.* **2012**, *31*, 70.

13 (27) Schmid-Rohl, A.; Rohl, H. J.; Oschmann, W.; Frimmel, A.;
14 Schwark, L. *Geobios* **2002**, *35*, 13.

15 (28) Schwark, L.; Frimmel, A. *Chemical Geology* **2004**, *206*, 231.

16 (29) Rohl, H. J.; Schmid-Rohl, A. In *Deposition of Organic-Carbon-Rich*
17 *Sediments: Models, Mechanisms, and Consequences*; Harris, N. B., Ed.; S E P M
18 - Soc Sedimentary Geology: Tulsa, 2005; Vol. 82, p 165.

19 (30) Munoz, Y. A.; Littke, R.; Brix, M. R. *Geofluids* **2007**, *7*, 335.

20 (31) Institution, B. S. *BS 733-2:1987: Pyknometers: Methods for*
21 *calibration and use of pyknometers*; BSI, 1987.

22 (32) Espitalie, J. *Rev. IFP* **1977**, *32*, 23.

23 (33) Hillier, S. In *Clay Mineral Cements in Sandstones*; Blackwell
24 Publishing Ltd.: 2009, p 213.

25 (34) Hillier, S. *Clay Min.* **1999**, *34*, 127.

26 (35) Leon, C. *Advances in Colloid and Interface Science* **1998**, *76*, 341.

27 (36) Lapierre, C.; Leroueil, S.; Locat, J. *Can. Geotech. J.* **1990**, *27*, 761.

28 (37) Heling, D. *Sedimentology* **1970**, *15*, 247.

29 (38) Lowell, S.; Shields, J. E. *Powder surface area and porosity*;
30 Chapman and Hall: London, New York, 1991.

31 (39) Lemmon, E. W.; Huber, M. L.; McLinden, M. O. *NIST Reference*
32 *Fluid Thermodynamic and Transport Properties - REFPROP*, U.S. Department
33 of Commerce, 2010.

34 (40) Span, R.; Wagner, W. *J. Phys. Chem. Ref. Data* **1996**, *25*, 1509.

35 (41) Span, R.; Lemmon, E. W.; Jacobsen, R. T.; Wagner, W.; Yokozeki,
36 A. *J. Phys. Chem. Ref. Data* **2000**, *29*, 1361.

37 (42) Setzmann, U.; Wagner, W. *J. Phys. Chem. Ref. Data* **1991**, *20*,
38 1061.

39 (43) van Krevelen, D.; Schuyer, J. *Coal science*; Elsevier, 1957.

40 (44) Wilhelms, A.; Larter, S. R.; Leythaeuser, D. *Org. Geochem.* **1991**,
41 *17*, 351.

42 (45) Laxminarayana, C.; Crosdale, P. J. *Int. J. Coal Geol.* **1999**, *40*, 309.

43 (46) Gurvitch, L. *J. Phys. Chem. Soc. Russ.* **1915**, *47*, 805.

44 (47) Marsh, H. *Carbon* **1987**, *25*, 49.

- 1
2
3 (48) Fletcher, A. J.; Thomas, K. M.; Rosseinsky, M. J. *Journal of Solid*
4 *State Chemistry* **2005**, *178*, 2491.
- 5
6 (49) Sing, K. S. W.; Everett, D. H.; Haul, R. A. W.; Moscou, L.; Pierotti,
7 R. A.; Rouquerol, J.; Siemieniewska, T. *Pure and Applied Chemistry* **1985**, *57*,
8 603.
- 9
10 (50) Garrido, J.; Linares-Solano, A.; Martin-Martinez, J. M.; Molina-
11 Sabio, M.; Rodriguez-Reinoso, F.; Torregrosa, R. *Langmuir* **1987**, *3*, 76.
- 12 (51) Marsh, H.; Wynne-Jones, W. F. K. *Carbon* **1964**, *1*, 269.
- 13 (52) Sing, K. S. W.; Williams, R. T. *Particle & Particle Systems*
14 *Characterization* **2004**, *21*, 71.
- 15
16 (53) Lamond, T. G.; Metcalfe, J. E. I.; Walker, P. L. J. *Carbon* **1965**, *3*,
17 59.
- 18
19 (54) Rodriguez-Reinoso, F.; Linares-Solano, A. In *Chemistry and*
20 *Physics of Carbon*; Thrower, P. A., Ed.; New York: Marcel Dekker, 1989; Vol.
21 21, p 1.
- 22
23 (55) Cazorla-Amoros, D.; Alcaniz-Monge, J.; de la Casa-Lillo, M. A.;
24 Linares-Solano, A. *Langmuir* **1998**, *14*, 4589.
- 25 (56) *Handbook of Compressed Gases, 3rd Edition Van Nostrand*
26 *Reinhold, New York 1990*; 3rd ed.; Van Nostrand Reinhold: New York, 1990.
- 27 (57) Firouzi, M.; Rupp, E. C.; Liu, C. W.; Wilcox, J. *Int. J. Coal Geol.*
28 **2014**, *121*, 123.
- 29
30 (58) Krooss, B. M.; van Bergen, F.; Gensterblum, Y.; Siemons, N.;
31 Pagnier, H. J. M.; David, P. *Int. J. Coal Geol.* **2002**, *51*, 69.
- 32 (59) Xiao, B.; Wheatley, P. S.; Zhao, X.; Fletcher, A. J.; Fox, S.; Rossi, A.
33 G.; Megson, I. L.; Bordiga, S.; Regli, L.; Thomas, K. M.; Morris, R. E. *J. Am.*
34 *Chem. Soc.* **2007**, *129*, 1203.
- 35
36 (60) Lin, X.; Telepeni, I.; Blake, A. J.; Dailly, A.; Brown, C. M.; Simmons,
37 J. M.; Zoppi, M.; Walker, G. S.; Thomas, K. M.; Mays, T. J.; Hubberstey, P.;
38 Champness, N. R.; Schroder, M. *J. Am. Chem. Soc.* **2009**, *131*, 2159.
- 39 (61) Furukawa, H.; Miller, M. A.; Yaghi, O. M. *J. Mater. Chem.* **2007**, *17*,
40 3197.
- 41
42 (62) Murray, L. J.; Dinca, M.; Long, J. R. *Chem. Soc. Rev.* **2009**, *38*,
43 1294.
- 44
45 (63) Broom, D. P.; Thomas, K. M. *MRS Bull.* **2013**, *38*, 412.
- 46 (64) Ambrose, R. J.; Hartman, R. C.; Diaz-Campos, M.; Akkutlu, I. Y.;
47 Sondergeld, C. H. *Spe J.* **2012**, *17*, 219.
- 48 (65) Ji, L. M.; Zhang, T. W.; Milliken, K. L.; Qu, J. L.; Zhang, X. L. *Appl.*
49 *Geochem.* **2012**, *27*, 2533.
- 50 (66) Liu, D.; Yuan, P.; Liu, H. M.; Li, T.; Tan, D. Y.; Yuan, W. W.; He, H.
51 P. *Applied Clay Science* **2013**, *85*, 25.
- 52
53 (67) Sircar, S. *Ind. Eng. Chem. Res.* **1992**, *31*, 1813.
- 54 (68) Myers, A. L.; Monson, P. A. *Langmuir* **2002**, *18*, 10261.
- 55
56
57
58
59
60

- 1
2
3 (69) Cole, J. H.; Everett, D. H.; Marshall, C. T.; Paniago, A. R.; Powl, J.
4 C.; Rodriguez-Reinoso, F. J. *Chem. Soc. Faraday Trans.* **1974**, *70*, 2154.
5 (70) Czepirski, L.; Jagiello, J. *Chem. Eng. Sci.* **1989**, *44*, 797.
6 (71) Himeno, S.; Komatsu, T.; Fujita, S. J. *Chem. Eng. Data* **2005**, *50*,
7 369.
8 (72) Duren, T.; Sarkisov, L.; Yaghi, O. M.; Snurr, R. Q. *Langmuir* **2004**,
9 *20*, 2683.
10 (73) Rahman, K. A.; Loh, W. S.; Yanagi, H.; Chakraborty, A.; Saha, B. B.;
11 Chun, W. G.; Ng, K. C. J. *Chem. Eng. Data* **2010**, *55*, 4961.
12 (74) Ruppel, T. C.; Grein, C. T.; Bienstoc.D *Fuel* **1974**, *53*, 152.
13 (75) Xia, X. Y.; Tang, Y. C. *Geochim. Cosmochim. Acta* **2012**, *77*, 489.
14 (76) Gurdal, G.; Yalcin, M. N. *Int. J. Coal Geol.* **2001**, *48*, 133.
15 (77) Clarkson, C. R.; Bustin, R. M. *Fuel* **1996**, *75*, 1483.
16 (78) Clarkson, C. R.; Bustin, R. M.; Levy, J. H. *Carbon* **1997**, *35*, 1689.
17 (79) Levine, J. R. *Coalification: The Evolution of Coal as Source Rock*
18 *and Reservoir Rock for Oil and Gas*; AAPG, 1993.
19 (80) Mosher, K.; He, J.; Liu, Y.; Rupp, E.; Wilcox, J. *Int. J. Coal Geol.*
20 **2013**, *109–110*, 36.
21 (81) Cai, Y. D.; Liu, D. M.; Pan, Z. J.; Yao, Y. B.; Li, J. Q.; Qiu, Y. K. *Fuel*
22 **2013**, *103*, 258.
23 (82) Sing, K. *Colloids and Surfaces A: Physicochemical and*
24 *Engineering Aspects* **2001**, *187–188*, 3.
25 (83) Mahajan, O. P. *Carbon* **1991**, *29*, 735.
26
27
28
29
30
31
32
33
34
35
36
37
38
39
40
41
42
43
44
45
46
47
48
49
50
51
52
53
54
55
56
57
58
59
60

1
2
3 **Figures and Tables**
4

5 **Table 1: Well depth, TOC, grain and helium densities, mercury injection pore volumes and**
6 **total porosities for Posidonia shales and kerogens.**
7

8
9
10
11
12
13
14
15
16
17
18
19
20
21
22
23
24
25
26
27
28
29

Well	Sample	Depth	TOC	Shale grain density	Shale density (Helium Pycnometry)	Shale Bulk Vol. (MICP)	Shale Total Pore Vol.	Kerogen TOC†	Kerogen density (Helium Pycnometry)
		[m]	[wt%]	[g cm ⁻³]	[g cm ⁻³]	[cm ³ g ⁻¹]	[%]	[wt%]	[g cm ⁻³]
WIC	7145	47.4	10.92	2.331	2.321	0.497	13.8	73	1.217
WIC	7155	57.8	9.67	2.361	2.297	0.484	12.5	73	1.235
HAR	7038	44.5	7.91	2.493	2.468	0.414	3.1	97	1.168
HAR	7060	66.8	5.78	2.592	2.550	0.404	4.5	>99	1.024
HAD	7090	40.1	7.41	2.572	2.556	0.439	11.4	83	1.342
HAD	7119	60.6	7.15	2.607	2.614	0.445	13.7	79	1.368

30 † The kerogen TOC content is corrected for the residual pyrite content, which could not be
31 removed by the separation process.
32
33
34
35
36
37
38
39
40
41
42
43
44
45
46
47
48
49
50
51
52
53
54
55
56
57
58
59
60

Table 2: Rock-Eval pyrolysis results for Posidonia shales

	S1	S2	T _{MAX}	PP	PI	HI
	[mg g ⁻¹]	[mg g ⁻¹]	[°C]	[mg g ⁻¹]		[mg _{HC} g _{TOC} ⁻¹]
WIC7145	4.2	72.0	425	76.2	0.05	660
WIC7155	3.9	69.4	429	73.3	0.05	718
HAR7038	3.3	30.2	449	33.5	0.10	382
HAR7060	2.0	21.2	447	23.2	0.09	361
HAD7090	0.9	4.2	464	5.1	0.18	56
HAD7119	1.2	3.2	459	4.4	0.28	44

S1 = Free hydrocarbon

S2 = Generated hydrocarbon through thermal cracking of non-volatile organic matter

T_{MAX} = Temperature of maximum release of cracked hydrocarbons

PP = Production Potential

PI = Production Index

HI = Hydrogen Index

Table 3: Mineral composition of Posidonia shales in wt%. Other minerals includes Feldspar, Siderite, Anatase, Marcasite, Aragonite and Dickite (not more than 1.5 wt%)

	Quartz	Plagioclase	Calcite	Dolomite	Pyrite	Gypsum	Muscovite	Illite + I-S	Kaolinite	Chlorite	Other
WIC7145	13.2	1.0	46.6	0.3	3.9	2.2	0.0	22.4	5.1	2.0	3.3
WIC7155	8.6	1.4	55.3	0.6	5.4	2.4	0.1	19.4	2.2	1.8	2.8
HAR7038	15.8	2.1	43.5	0.7	5.6	0.0	3.2	18.5	8.9	0.0	1.7
HAR7060	13.0	2.8	30.5	6.4	9.1	0.0	3.7	26.2	6.6	0.0	1.7
HAD7090	16.0	3.0	39.7	1.8	5.0	1.8	1.3	23.9	3.9	0.7	2.9
HAD7119	8.2	4.9	49.9	2.7	4.5	3.8	0.0	19.5	1.1	2.7	2.7

Table 4: Shale and kerogen pore volumes measured by different techniques.

Sample	Pore Diameter Range [nm]							BET Surface Area
	< 0.7	< 1.5	0.3 – 2		6-1093		SPV+ MICP	
	CO ₂ (0°C) UMP	CO ₂ (0°C) NLDFT	N ₂ (-196°C) MPV	CO ₂ (-78°C) SPV	MICP	TPV		
	mm ³ g ⁻¹							
Shale								
WIC7145	6.7	4.6	2.9	16.4	53.1	68.4	69.5	6.7
WIC7155	8.0	7.7	1.6	15.5	48.1	60.7	63.6	4.3
HAR7038	5.2	4.3	-	8.4	5.1	12.7	13.5	-
HAR7060	4.6	5.7	-	8.3	7.8	18.1	16.1	-
HAD7090	6.4	6.0	11.6	16.2	26.0	50.1	42.2	25.1
HAD7119	6.0	4.0	9.1	13.0	45.1	61.1	58.1	21.0
Kerogen								
WIC7145	32.5	21.8	5.2	74.8				12.5
WIC7155	28.8	24.3	3.7	71.8				7.5
HAR7038	27.0	25.3	11.9	68.5				27.3
HAR7060	33.5	33.1	9.0	87.0				17.9
HAD7090	50.6	42.4	34.6	113.0				68.1
HAD7119	54.6	50.8	24.2	103.6				56.1

UMP = Ultramicropore Volume determined using the DR equation and CO₂ sorption at 0°C; NLDFT = Pore volume determined by applying a Non-Local Density Functional Theory model to Carbon Dioxide 0°C isotherms, N₂ MPV = Micropore volume determined by the D R equation from -196°C nitrogen isotherms; SPV = Sorption pore volume based on Gurvitch's Rule and calculated from CO₂ isotherms at -78°C; MICP = Pore Volume from mercury injection capillary pressure porosimetry, the estimated pore constriction sizes were derived from Washburn equation (see Supporting Information); TPV = Total pore volume from equation (2) using mercury bulk density and Grain Density/Helium Pycnometry (skeletal volume); Total Porosity = 1 – Mercury bulk density/(Grain or He density), equation (3); SPV+MICP = sum of CO₂ -78°C sorption pore volume and MICP pore volume, equation (4).

Table 5: Parameters calculated by fitting the Langmuir equation to the shale methane sorption data.

Sample	Shale					Kerogen			
	ρ_{ad}	K(45)	K(65)	K(85)	Error	ρ_{ad}	K(45)	K(65)	Error
	kg m ⁻³	MPa ⁻¹				kg m ⁻³	MPa ⁻¹		
WIC 7145	371	0.112	0.087	0.068	1.3E-04	478	0.058	0.048	2.0E-03
WIC 7155	388	0.099	0.077	0.061	8.5E-05	503	0.057	0.040	2.7E-03
HAR 7038	415	0.102	0.074		3.2E-05	516	0.064	0.048	2.0E-03
HAR 7060	340	0.115	0.084		4.7E-06	441	0.069	0.047	4.5E-03
HAD 7090	293	0.193	0.152	0.118	1.5E-04	356	0.118	0.089	9.6E-03
HAD 7119	299	0.188	0.147	0.114	8.1E-05	614	0.054	0.040	4.5E-02

The error column shows the accumulated error (residuals sum of squares) of the fit. The adsorbed phase density is assumed to be constant over the (relatively small) temperature range.

Table 6: Isothermic Enthalpies of Adsorption of CH₄ on shales and kerogens at zero surface coverage ($Q_{st,n=0}$).

Calculation Method	Shale $Q_{st,n=0}$ (kJ mol ⁻¹)					
	WIC 7145	WIC 7155	HAR7038	HAR7060	HAD7090	HAD7119
1. Virial	15.1 ± 0.1	15.7 ± 2.8	11.8 ± 0.4	12.9 ± 2.4	15.7 ± 0.8	15.4 ± 0.1
3. Monson & Myers	11.7 ± 0.1	11.2 ± 0.4	14.0 ± 0.5	12.7 ± 1.9	11.7 ± 0.1	12.1 ± 0.3
Kerogen $Q_{st,n=0}$ (kJ mol ⁻¹)						
1. Virial	11.2		14.5	12.8	15.7	11.5
2. Myers & Monson	8.5 ± 1.3	15.8 ± 2.8	12.9	17.2 ± 1.4	12.6 ± 1.7	13.4 ± 0.8

1: The Virial equation was used to calculate the enthalpy at zero surface coverage (ZSC) $Q_{st,n=0}$ from the absolute isotherm. 2: The method of Myers and Monson was used to calculate $Q_{st,n=0}$. Kerogen WIC7155: sorption data did not give a suitable fit to the Virial equation.

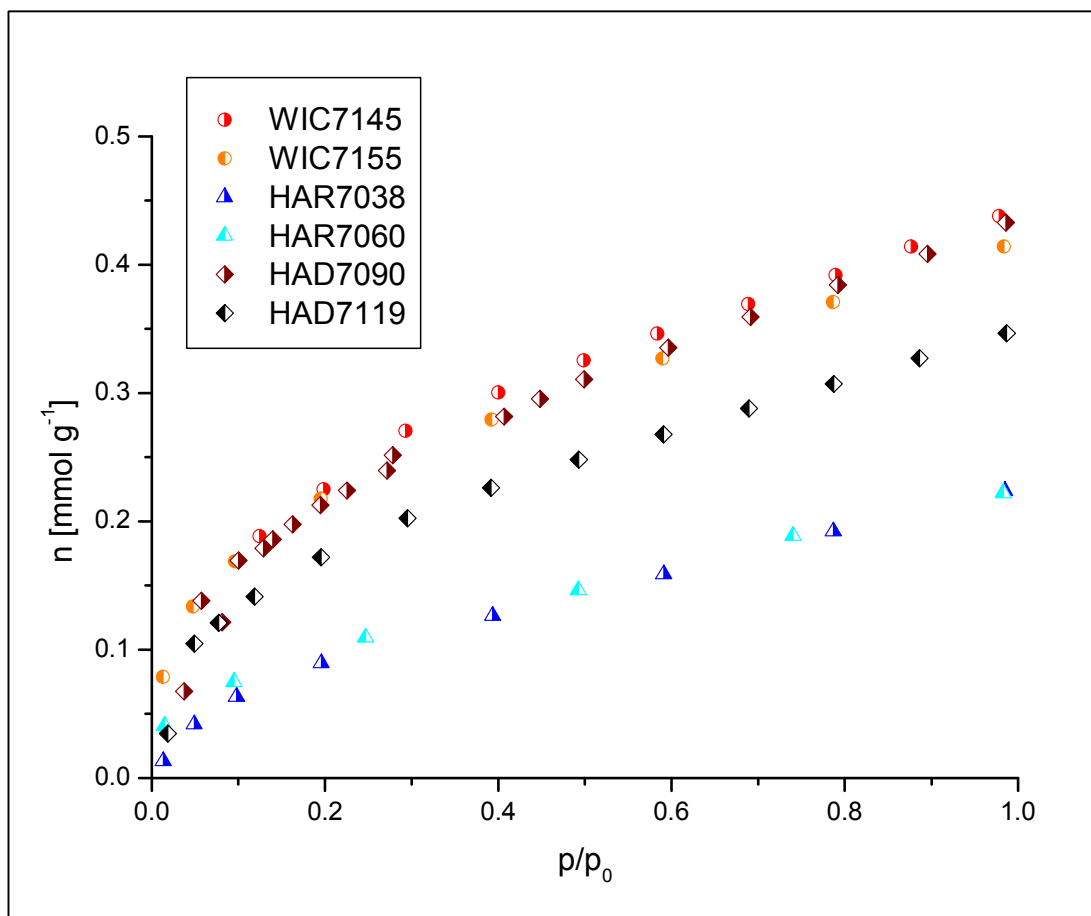


Figure 1: CO₂ adsorption isotherms for shales at -78°C.

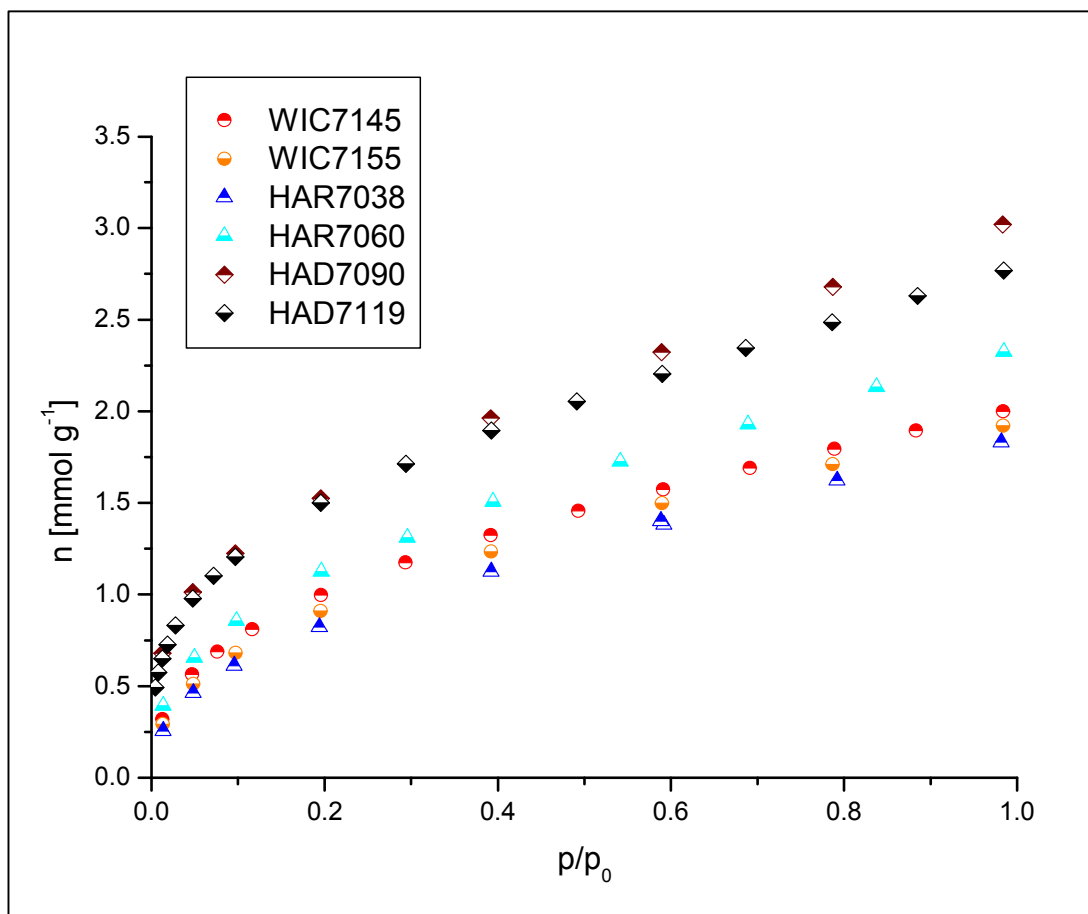


Figure 2: CO₂ isotherms for kerogens at -78°C.

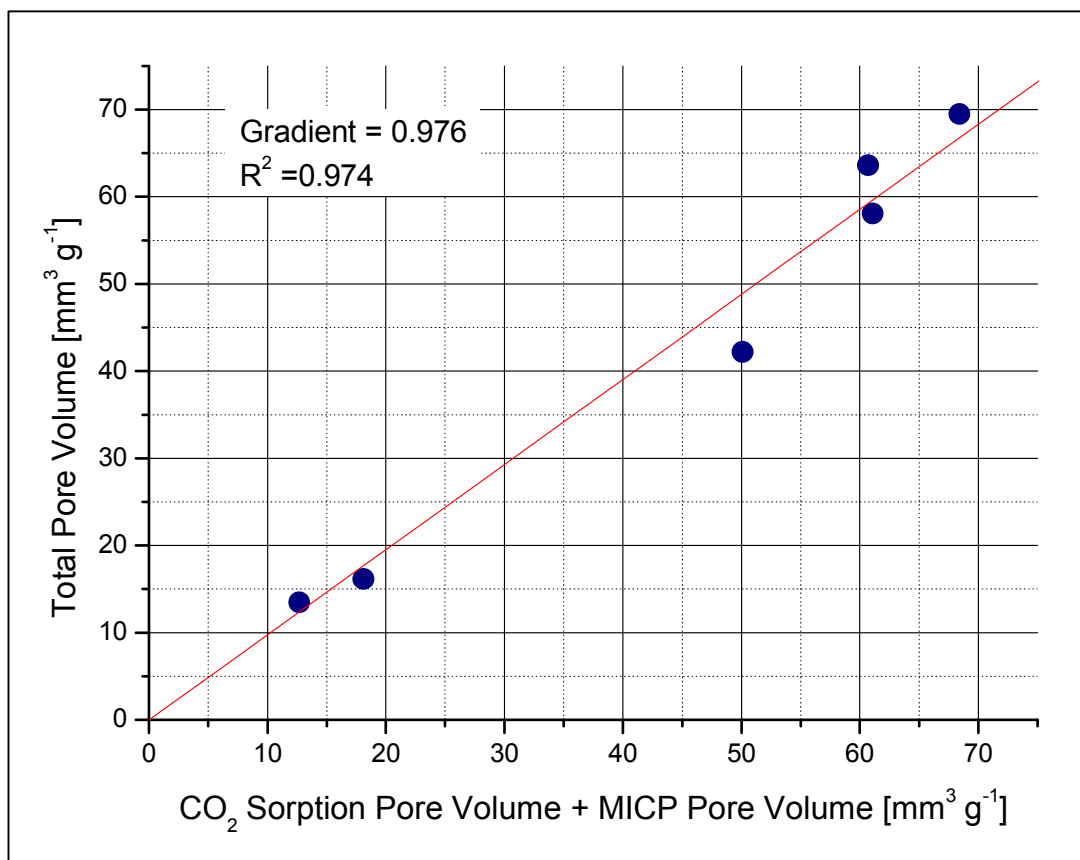


Figure 3: Correlation of Total Pore Volume with CO₂ Sorption Pore Volume(-78°C) plus MICP Pore Volume. Pore Volumes were calculated assuming an adsorbed phase density of 1.177 g cm⁻³.

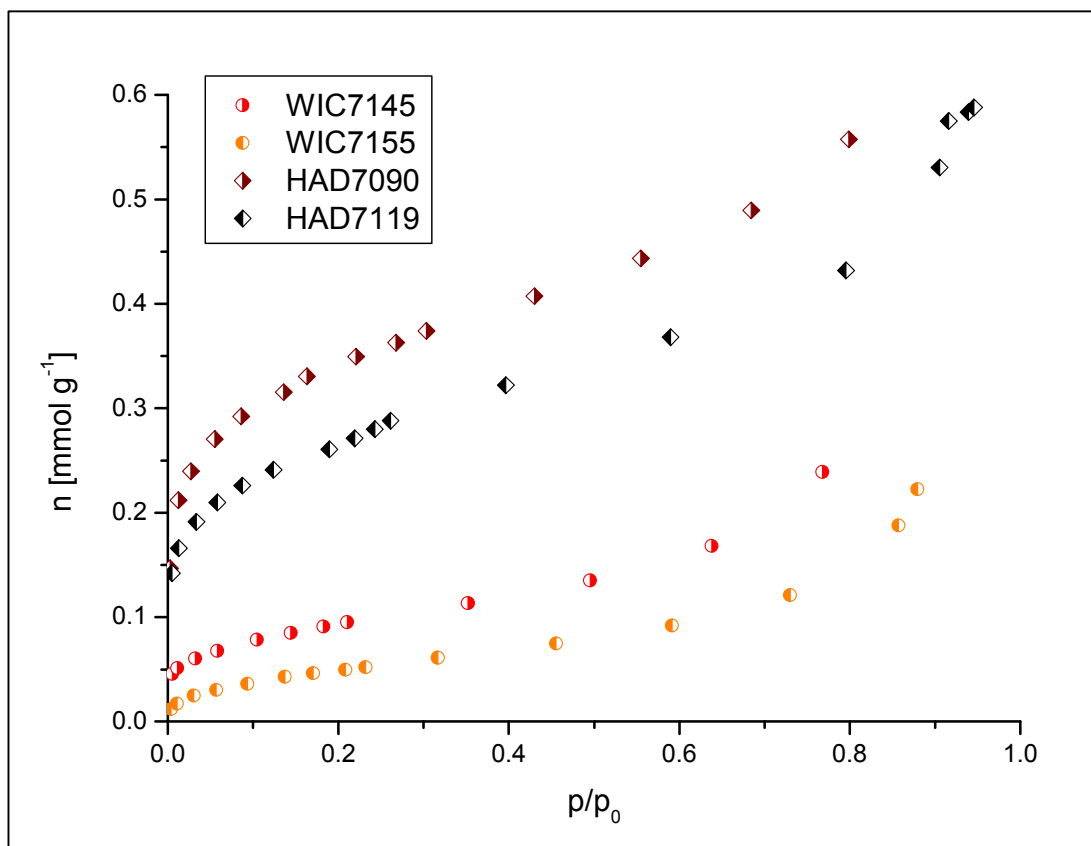


Figure 4: N₂ adsorption isotherms at -196°C for Posidonia shales.

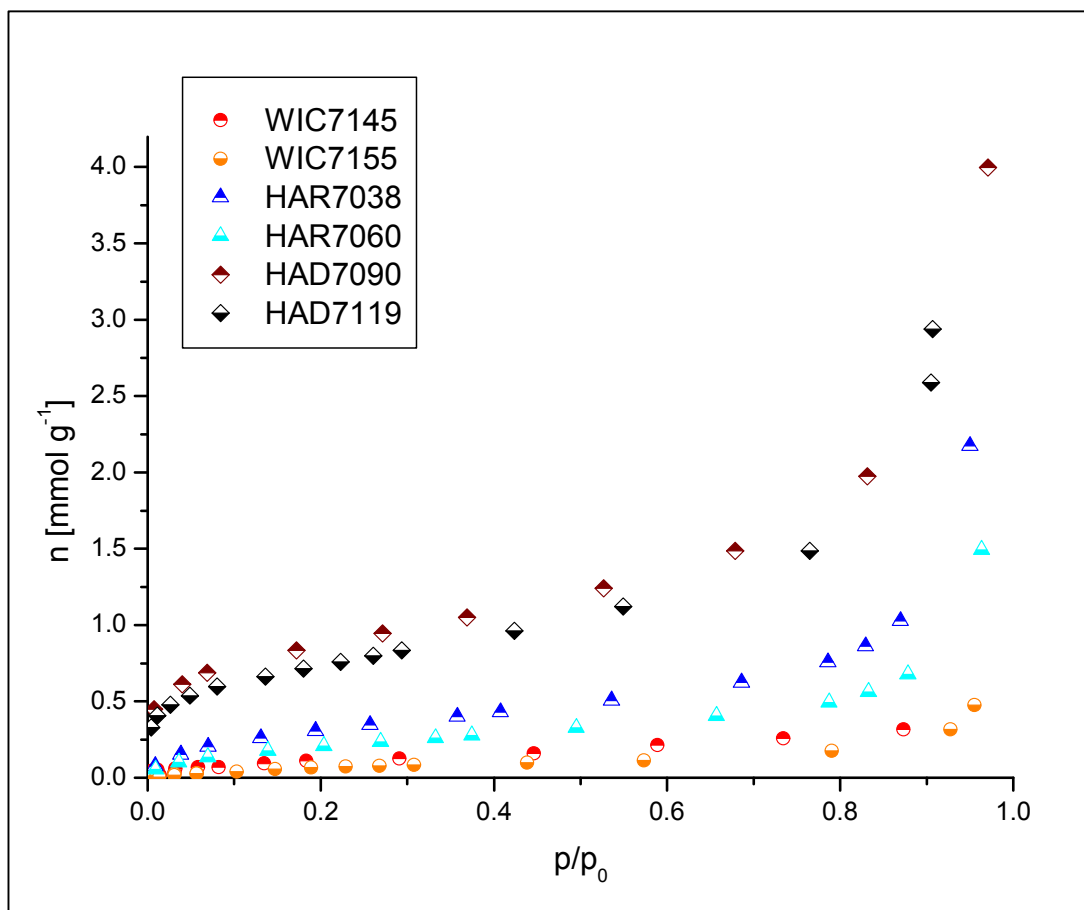


Figure 5: N₂ adsorption isotherms at -196°C for Posidonia kerogens.

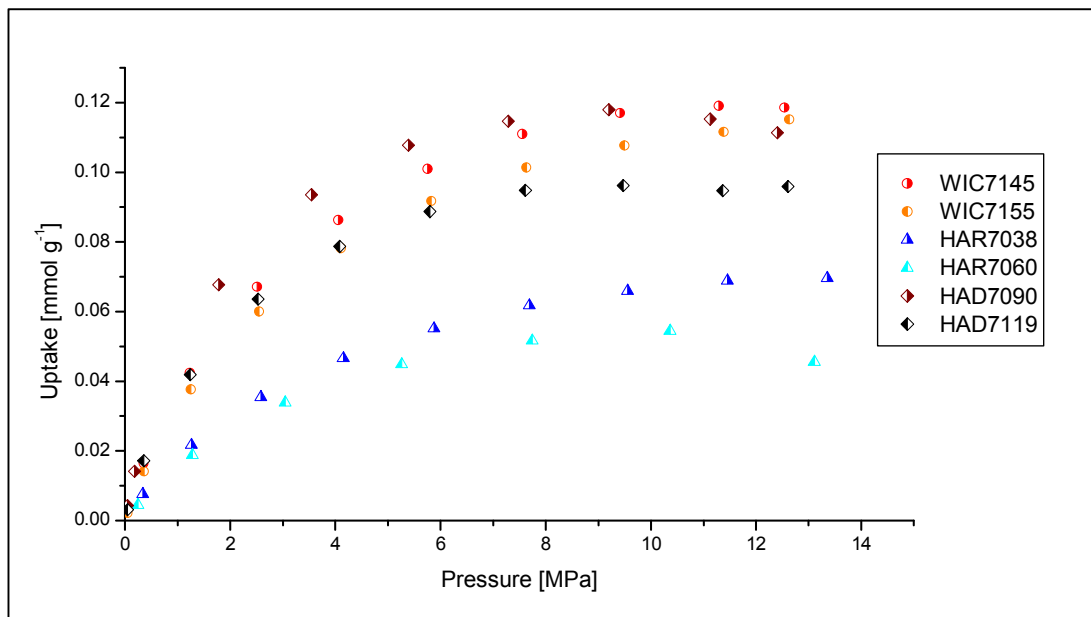


Figure 6: Methane surface excess adsorption isotherms at 45°C on Posidonia shales

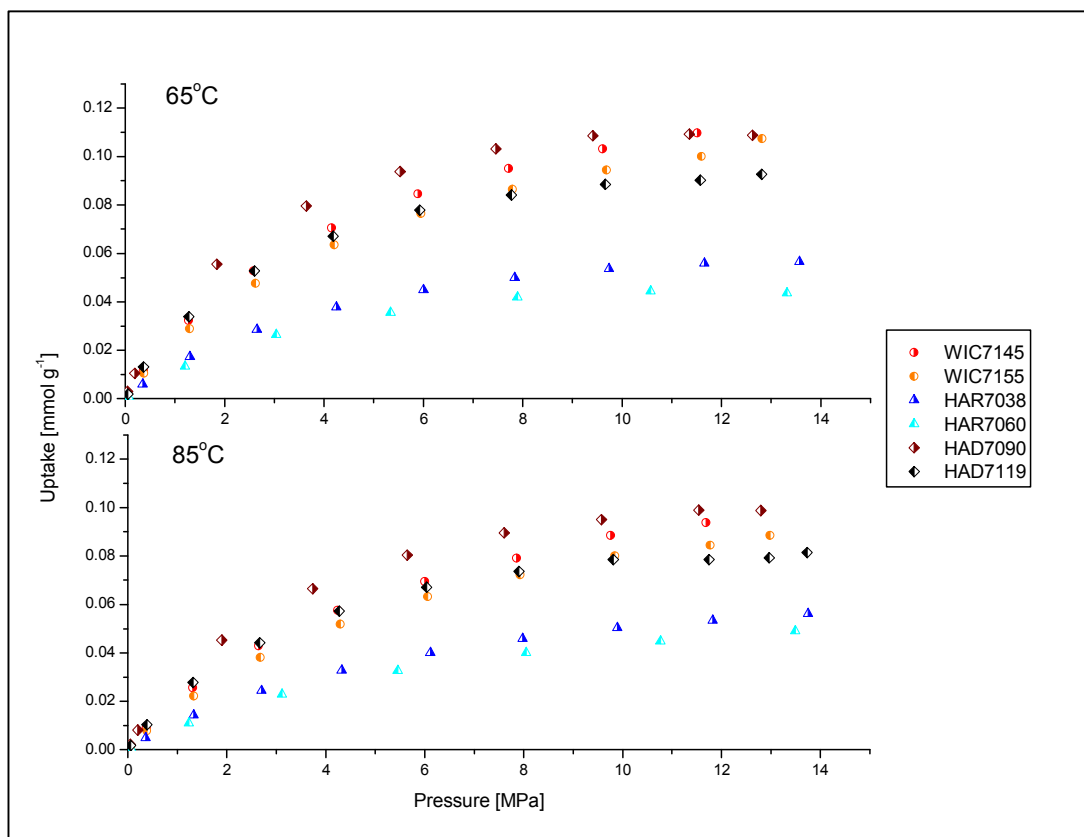


Figure 7: Methane surface excess adsorption isotherms at 65°C and 85°C on Posidonia shales.

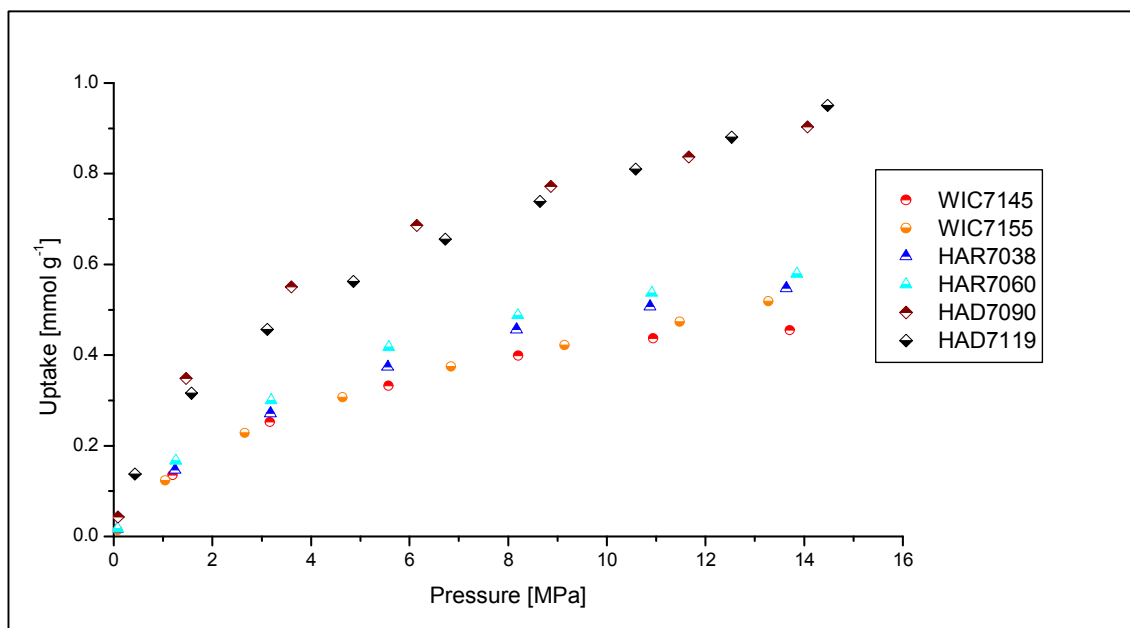


Figure 8: Methane surface excess isotherms for Posidonia kerogens at 45°C.

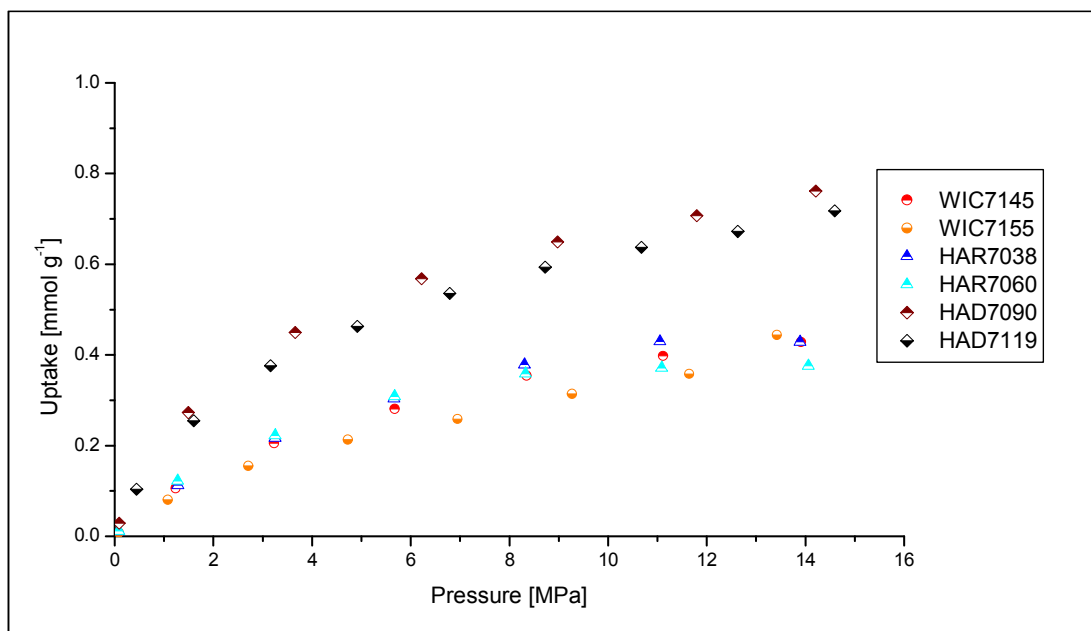


Figure 9: Methane surface excess adsorption isotherms for Posidonia kerogens at 65°C.

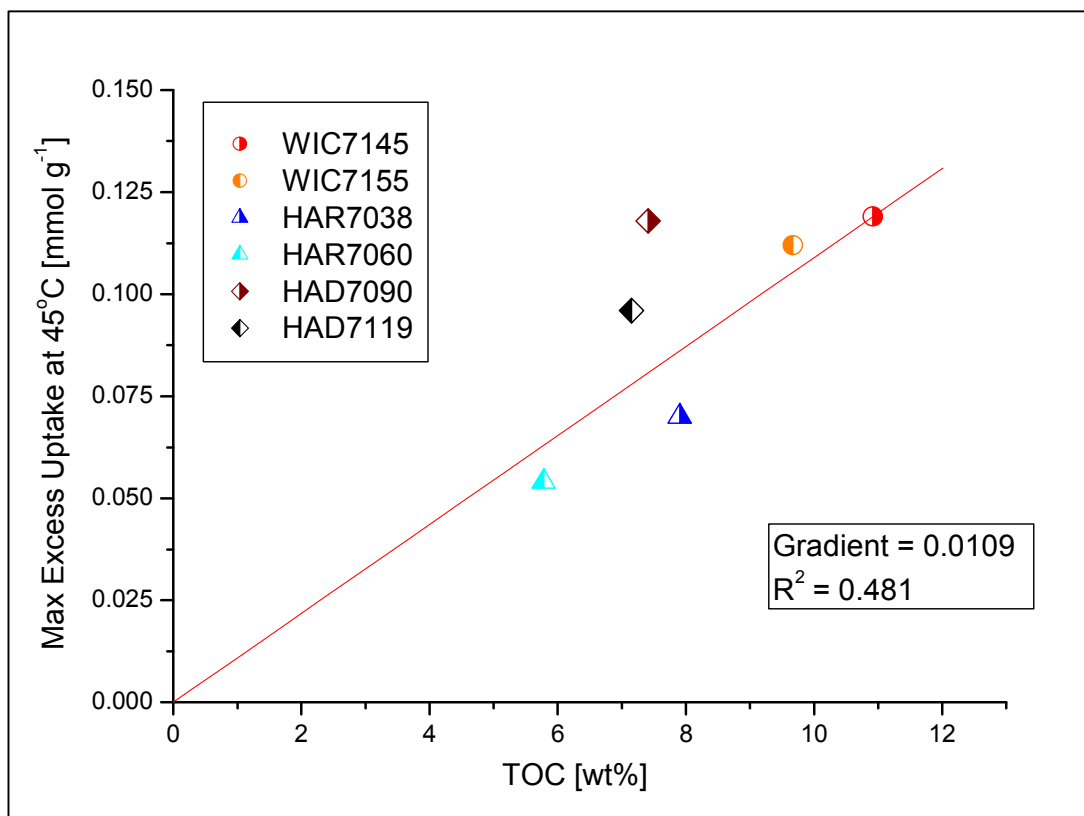


Figure 10: Plot of Maximum methane surface excess uptake at 45°C versus TOC.

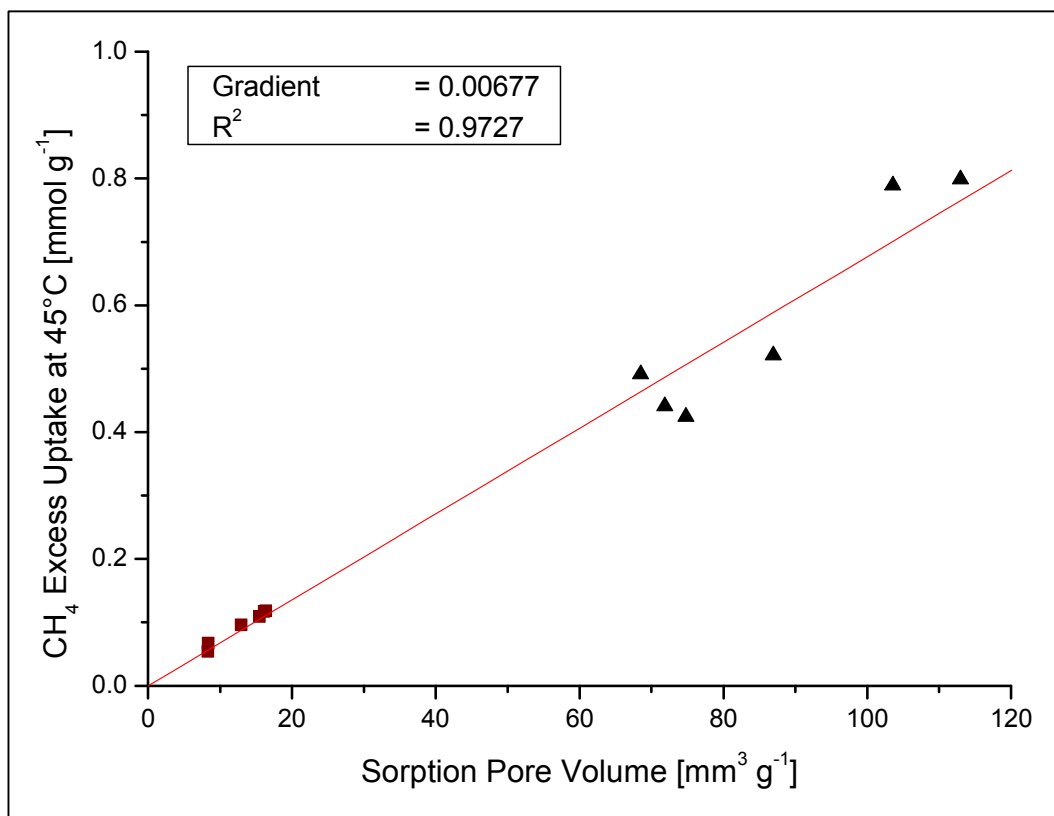


Figure 11: Graph of CH₄ maximum excess uptake at 45°C and 10 MPa on shale (squares) and kerogen (triangles) versus CO₂ sorption pore volume (-78°C).

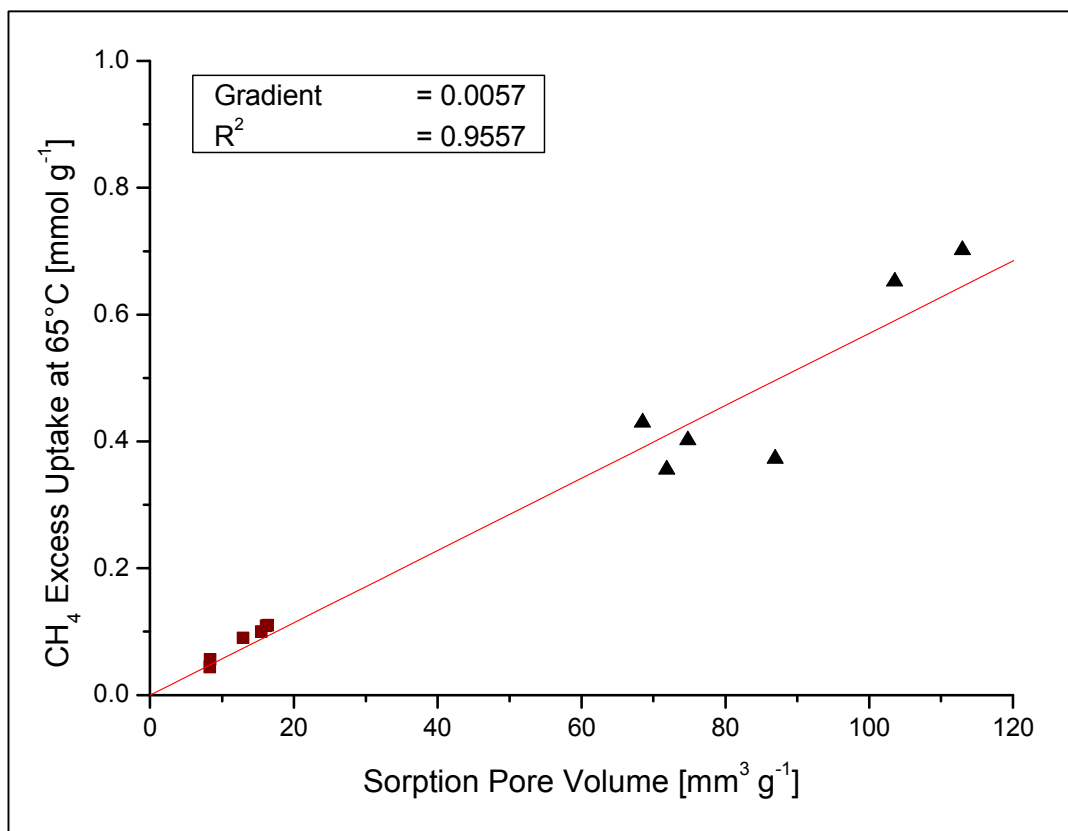


Figure 12: Graph of CH₄ excess uptake at 65°C and 11.5 MPa on shale (squares) and kerogen (triangles) versus CO₂ sorption pore volume (-78°C).

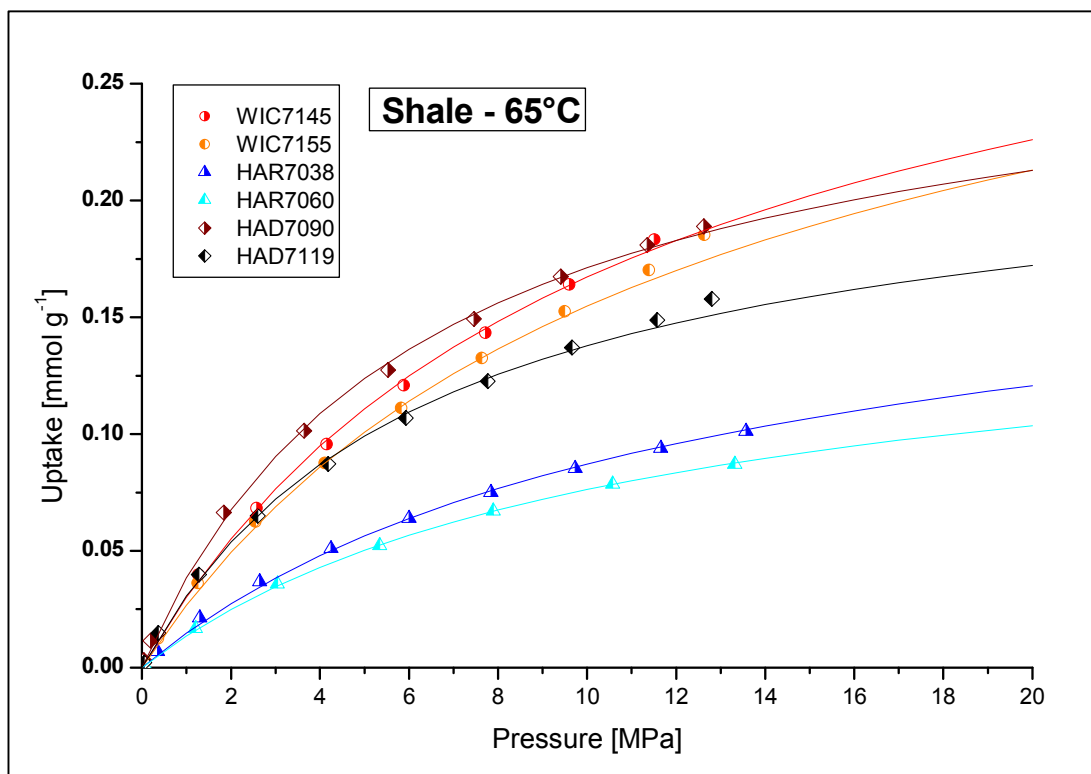


Figure 13: Absolute methane isotherms on shale at 65°C. It is assumed that the volume of the adsorbed phase is equal to the CO₂ sorption pore volume. The lines represent the Langmuir fit to the absolute and excess data (simultaneous fit).

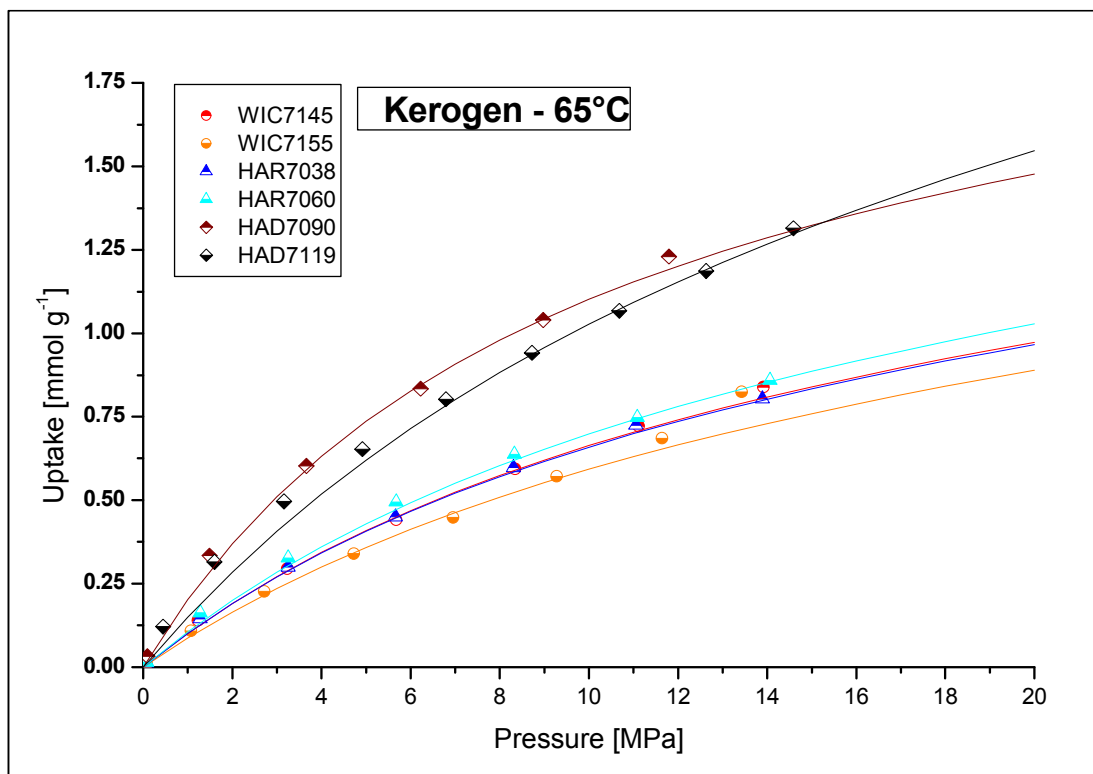


Figure 14: Absolute methane isotherms on kerogen at 65°C. It is assumed that the volume of the adsorbed phase is equal to the CO₂ sorption pore volume. The lines represent the Langmuir fit to the absolute and excess data (simultaneous fit).

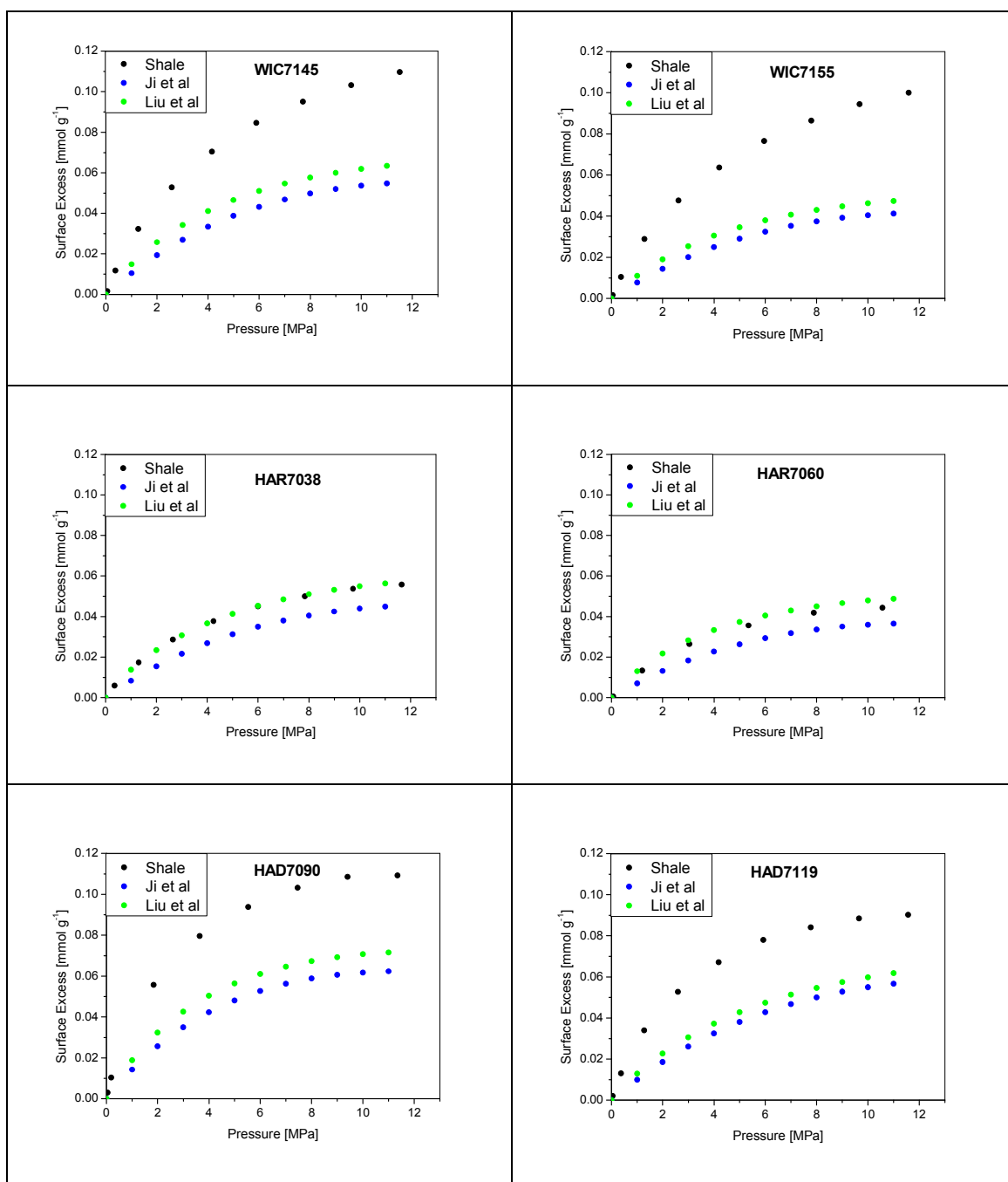


Figure 15: Mass balances of methane surface excess sorption on shale at 65°C. The experimental shale excess isotherms (black) are compared to mass balance isotherms calculated from the sorption excess data for kerogen, TOC and mineral composition determined in this study and sorption data for clay minerals reported by Ji et al⁶⁵ (blue) and Liu et al (green).⁶⁶ The isotherms were obtained by fitting kerogen and clay mineral data to the Langmuir equation and components were normalized and summed for comparisons with the experimental shale isotherms.

1
2
3
4
5
6
7
8
9
10
11
12
13
14
15
16
17
18
19
20
21
22
23
24
25
26
27
28
29
30
31
32
33
34
35
36
37
38
39
40
41
42
43
44
45
46
47
48
49
50
51
52
53
54
55
56
57
58
59
60

Table of Contents Graphic